J Neurophysiol 105: 1276–1294, 2011.
First published January 5, 2011; doi:10.1152/jn.00792.2010.

Inhibition of SK and M channel-mediated currents by 5-HT enables parallel processing by bursts and isolated spikes

Tara Deemyad,[1] Leonard Maler,[2,3] and Maurice J. Chacron[1,4]

[1]*Department of Physiology, McGill University, Montreal, Quebec;* [2]*Department of Cellular and Molecular Medicine and* [3]*Center for Neural Dynamics, University of Ottawa, Ottawa, Ontario; and* [4]*Department of Physics, McGill University, Montreal, Quebec, Canada*

Submitted 15 September 2010; accepted in final form 3 January 2011

Deemyad T, Maler L, Chacron MJ. Inhibition of SK and M channel-mediated currents by 5-HT enables parallel processing by bursts and isolated spikes. *J Neurophysiol* 105: 1276–1294, 2011. First published January 5, 2011; doi:10.1152/jn.00792.2010.—Although serotonergic innervation of sensory brain areas is ubiquitous, its effects on sensory information processing remain poorly understood. We investigated these effects in pyramidal neurons within the electrosensory lateral line lobe (ELL) of weakly electric fish. Surprisingly, we found that 5-HT is present at different levels across the different ELL maps; the presence of 5-HT fibers was highest in the map that processes intraspecies communication signals. Electrophysiological recordings revealed that 5-HT increased excitability and burst firing through a decreased medium afterhyperpolarization resulting from reduced small-conductance calcium-activated (SK) currents as well as currents mediated by an M-type potassium channel. We next investigated how 5-HT alters responses to sensory input. 5-HT application decreased the rheobase current, increased the gain, and decreased first spike latency. Moreover, it reduced discriminability between different stimuli, as quantified by the mutual information rate. We hypothesized that 5-HT shifts pyramidal neurons into a burst-firing mode where bursts, when considered as events, can detect the presence of particular stimulus features. We verified this hypothesis using signal detection theory. Our results indeed show that serotonin-induced bursts of action potentials, when considered as events, could detect specific stimulus features that were distinct from those detected by isolated spikes. Moreover, we show the novel result that isolated spikes transmit more information after 5-HT application. Our results suggest a novel function for 5-HT in that it enables differential processing by action potential patterns in response to current injection.

serotonin; neuromodulator; information theory; weakly electric fish; feature detection

EFFICIENT AND ADAPTIVE PROCESSING of behaviorally relevant sensory stimuli is essential for survival and can be accomplished by dynamically regulating sensory neuron tuning to these stimuli. Such regulation is in part implemented by neuromodulators such as serotonin (5-HT). There are massive serotonergic projections from the Raphe nuclei to almost every part of the mammalian brain, including sensory areas such as thalamus and cortex (see Berger et al. 2009 for review). However, their functional role in sensory processing is not well understood, in part because previous studies have shown that 5-HT could have opposite effects within the same brain area (Foehring et al. 2002; Hurley et al. 2004; Hurley and Pollak 2005a; Waterhouse et al. 1986, 1990; Yuan et al. 2003). This is due to different mechanisms of action by 5-HT at the cellular level (Beique et al. 2004, 2007; Bohorquez and Hurley 2009; Foehring et al. 2002; Hurley 2006; Hurley et al. 2004; Shen et al. 2007; Villalobos et al. 2004, 2005). Studies performed in model organisms whose sensory neural architecture is well-characterized anatomically, behaviorally, and physiologically are likely to speed progress toward a general understanding of altered sensory information processing by 5-HT and its consequences on behavior.

The electrosensory system of weakly electric fish displays many similarities with mammalian sensory systems (Krahe and Gabbiani 2004; Sadeghi et al. 2007) and benefits from well-characterized anatomy (Bell and Maler 2005) and physiology (Berman and Maler 1998a,b,c; Maler 2007, 2009a,b). Through an array of specialized tuberous electroreceptors on their skin, these fish sense amplitude modulations of their self-generated electric field (Turner et al. 1999). These electroreceptors synapse onto pyramidal neurons within the electrosensory lateral line lobe (ELL) (Bell and Maler 2005) whose physiology has been well characterized both in vitro and in vivo (see Maler 2009a,b for review). There are two types of pyramidal cells: basilar and nonbasilar cells (Maler 1979; Maler et al. 1981), which also are referred to as E- and I-cells because they respond to increased electric organ discharge (EOD) amplitude with excitation and inhibition, respectively (Saunders and Bastian 1984), and are functionally equivalent to the on and off cells found in the retina and lateral geniculate nucleus (Maler et al. 1981). Recent studies have found differences between the frequency tuning of E- and I-cells: whereas I-cells are tuned to low frequencies, E-cells are tuned to higher frequencies (Chacron et al. 2005; Krahe et al. 2008). Both E- and I-type pyramidal neurons receive massive synaptic input from higher electrosensory centers on their elaborate apical dendritic trees, which extend into the ELL molecular layers (Sas and Maler 1983, 1987). Previous studies demonstrated multiple roles for these descending inputs, including gain control (Bastian 1986a,b) and modulation of frequency tuning (Bastian et al. 2004; Chacron et al. 2005).

The ELL is composed of four parallel maps of the body surface, three of which receive identical tuberous electroreceptor input (Carr et al. 1982; Heiligenberg and Dye 1982; Shumway 1989a,b). These maps have been shown to mediate different behaviors (Metzner and Juranek 1997): in particular, the lateral map is involved in the processing of communication signals (Krahe et al. 2008; Marsat and Maler 2010; Marsat et al. 2009; Shumway 1989a) associated with aggressive behavior (Hupe et al. 2008; Zakon et al. 2002). Previous studies have

Address for reprint requests and other correspondence: M. J. Chacron, 3655 Sir William Osler, Rm. 1137, Montreal, QC, Canada H3G 1Y6 (e-mail: maurice.chacron@mcgill.ca).

0022-3077/11 Copyright © 2011 the American Physiological Society

Downloaded from jn.physiology.org on March 25, 2011

shown that the tuning of pyramidal neurons within the maps is intrinsic (Mehaffey et al. 2008c) and originates in part from membrane conductances (Deng et al. 2005; Ellis et al. 2007b, 2008; Krahe et al. 2008). Although previous studies have shown that serotonergic fibers are present in ELL (Johnston et al. 1990), putative differences in their presence across the ELL maps and their effects on sensory processing are unknown. Using a combination of immunohistochemical and electrophysiological techniques, we investigated the mechanisms by which 5-HT alters the properties of ELL pyramidal neurons within the three tuberous maps and its consequences on sensory information processing.

MATERIALS AND METHODS

Animals

The weakly electric fish *Apteronotus leptorhynchus* was used exclusively in this study. Animals were obtained from local importers and were acclimated to the laboratory as per published guidelines (Hitschfeld et al. 2009). All experimental procedures were approved by both McGill University's and the University of Ottawa's Animal Care Committees.

Histology

Immunohistochemical localization of 5-HT was done using recently described very sensitive procedures (Smith and Combs 2008; Telgkamp et al. 2007). Fish ($n = 6$) were deeply anesthetized [0.2% 3-aminobenzoic acid ethylester (MS-222)] and transcardially perfused with saline followed by 4% paraformaldehyde in phosphate buffer (pH 7.3). After postfixation (48 h, 4°C), 50-μm sections through the ELL were cut and processed (free floating) for 5-HT immunoreactivity using a tyramide signal amplification method (TSA; Invitrogen/Molecular Probes, Carlsbad, CA); control sections incubated without the 5-HT antibody showed no labeling (data not shown). Sections were incubated for 48 h in a rabbit anti-serotonin IgG (1:40,000 dilution; ImmunoStar, Hudson, WI, catalog no. 20080, lot no. 428002) in blocking solution (TSA kit). Endogenous peroxidases were blocked by incubating sections in 80% methanol-saline containing 0.6% H_2O_2 [dilute the 100% H_2O_2 600 μl in 99.4 ml of methanol-saline solution for 1 h at room temperature (RT)]. After a brief rinse (0.1 M PBS, 40 min), sections were incubated in horseradish peroxidase-conjugated goat anti-rabbit IgG (TSA kit) diluted 1:200 in blocking solution for 1 h (RT). After a 20-min rinse in PBS, sections were placed in Alexa Fluor 488-conjugated tyramide (1:100; TSA kit) in amplification buffer (TSA kit) containing 0.0015% H_2O_2 for 20 min at RT in the dark. Sections were then rinsed in PBS and counterstained with red fluorescent Nissl reagent (Molecular Probes, catalog no. N-21482) at a concentration of 1:300 in saline for 20 min at RT. Sections were then rinsed, mounted, and coverslipped with Vectashield (Vector Laboratories, Burlingame, CA).

Sections were photographed on a Zeiss Axioscope 2. Minor adjustments were made to the image in Photoshop (Adobe Systems). The "level" operation was used (all images) to match the effective range of the input to the entire range of the output, and the brightness was increased for the image shown in Fig. 1*A*. For the color images (see Fig. 1, *C* and *D*), the brightness of the 5-HT (green) was decreased and that of the Nissl counterstain (red) increased to better visualize the small granular interneurons. The final images were assembled in Adobe Illustrator.

Preparation of Slices

Animals were anesthetized by completely immersing them in a pH-adjusted MS-222 solution and then respirated via a mouth tube during surgery. ELL slices (300–400 μm) were then prepared as described previously (Ellis et al. 2007a,b; Mehaffey et al. 2008a,c; Turner et al. 1994) and were maintained by constant perfusion (2–3 ml/min) of artificial cerebrospinal fluid (ACSF; composition in mM: 126 NaCl, 2.5 KCl, 1.2 NaH_2PO_4, 1.2 $MgCl_2$, 18 $NaHCO_3$, 2.4 $CaCl_2$, and 11 D-glucose), as well as superfusion with carbogen (5% CO_2-95% O_2).

Recording Procedures

Glass microelectrodes were pulled to a fine tip using a P-97 filament puller (Sutter Instruments) and were filled with 2 M K-acetate. These had typical resistances of 70–110 MΩ. Sharp intracellular recordings were made from the somata of pyramidal neurons in the lateral (LS, $n = 84$), centrolateral (CLS, $n = 7$), and centromedial (CMS, $n = 5$) segments of the ELL. Typical resting membrane potential values were −70 mV, consistent with previous studies (Berman and Maler 1998c). Pyramidal cell somata are contained within the pyramidal cell layer of the ELL, which can be easily identified in the slice preparation (Mathieson and Maler 1988) (see Fig. 2*A*). An Axoclamp 900A was used to amplify the recorded potential difference between the tip of the recording electrode and a ground wire placed in the bath, as well as to deliver current injection through the recording electrode. Data were acquired at 10 kHz using a Digidata 1440A and Clampex 9.0 software (Molecular Devices).

ELL pyramidal cells can have action potential thresholds as low as −69 mV (Mehaffey et al. 2008c), which is presumably due to the presence of persistent sodium currents (Berman and Maler 1998c; Doiron et al. 2003b). As such, small fluctuations in the membrane potential caused by residual synaptic input or the random openings of ion channels can cause action potential firing at rest. We therefore used DC current injection to maintain each cell just below its firing threshold. Typical values used were −0.5 nA and are consistent with previous studies (Mehaffey et al. 2008c). We henceforth refer to this holding current as the baseline holding current. All pharmacological agents were dissolved in ACSF. 5-HT (1 mM) and UCL-1684 (UCL; 100 μM) were focally ejected by a PicoSpritzer III (Parker Hannifin, Cleveland, OH) to the ELL dorsal molecular layer by using patch electrodes with 1- to 2-μm tip diameter as conventionally used in other studies (Ellis et al. 2007a,b; Mehaffey et al. 2008a,c; Turner et al. 1994). Because of the orientation of the slice with respect to the ACSF flow in the chamber, these pharmacological agents will reach both the ventral molecular and pyramidal cell layers (Ellis et al. 2007a,b). We note that previous studies have shown that concentrations of UCL ranging from 10 nM (Hosseini et al. 2001) to 10 μM (Gluais et al. 2005; Hilgers and Webb 2005) were sufficient to block >90% of SK channels (e.g., see Monaghan et al. 2004) when bath applied. Because previous studies have estimated a dilution factor of ~10 for drugs applied with a PicoSpritzer (Turner et al. 1994), the concentration of UCL used in this study was thus set within the upper range used in previous studies. It is therefore likely that 100 μM UCL application blocked most SK channels in ELL pyramidal neurons. The typical pressure used for the PicoSpritzer was 7–15 psi, and the ejection typically lasted 150 ms. We bath applied XE-991 and linopirdine because we found that it could take up to 45 min for these drugs to have an effect, which is consistent with previous studies (Yue and Yaari 2006). We used concentrations of 7 and 10 μM for XE-991 and linopirdine, respectively. All chemicals were obtained from Sigma (St. Louis, MO) except UCL, XE-991, and linopirdine, which were obtained from Tocris (Ellisville, MO).

Experiment Protocols and Data Analysis

Single depolarizing current steps. The spiking activities of pyramidal neurons were obtained during a current step of 0.5 nA from the baseline holding current that lasted 2 s. These were quantified by the mean firing rate (i.e., the number of spikes per unit time). Further-

Downloaded from jn.physiology.org on March 25, 2011

more, interspike interval (ISI) sequences were computed as the time intervals between consecutive spikes, and ISI probability densities were generated with 1-ms binwidth. The coefficient of variation (CV) was computed as the standard deviation-to-mean ratio of the ISI probability density. The burst fraction was defined as the proportion of ISIs that are <10 ms, which correspond to the range of ISIs that will give rise to dendritic failure (Ellis et al. 2007a,b; Oswald et al. 2004). This value also corresponds to the trough in the bimodal ISI distribution as plotted on a log-linear scale (Turner et al. 1994), which is frequently taken as the threshold to segregate bursts from isolated spikes (Doiron et al. 2003a).

Average action potential waveforms were generated to measure the afterhyperpolarization (AHP) following each action potential. The amplitude of fast, medium, and slow components of the AHP were measured as the differences between the baseline membrane potential value before a spike (i.e., the average membrane potential at 10–15 ms before the peak of the spike) and the membrane potential value measured at 5 ms, 10–40 ms, and 2 s after the action potential peak, respectively (Faber and Sah 2002; Koyama and Appel 2006). We only considered action potentials that were "isolated" (i.e., that were not immediately preceded or followed by other action potentials) to estimate the full length of the AHP.

Multiple positive current steps. We used a set of 10 current steps, each lasting 1 s and ranging from 0.05 to 0.5 nA above the baseline holding current. We then measured the mean firing rate during each step. The mean firing rate was then plotted as a function of the current value minus the baseline value to obtain the frequency as a function of current (*f-I*) curve. The gain and rheobase (i.e., the minimum current needed to elicit spiking activity) were determined from the slope and *x*-intercept of the best linear fit to the *f-I* curve, respectively (Mehaffey et al. 2005).

Single negative current step. Negative current injections (−0.4 nA from the baseline holding current, 300-ms duration) were used to measure the subthreshold membrane resistance. Specifically, the membrane resistance was computed from Ohm's law using the deflection in membrane potential obtained in response to these current steps.

Random noise current. Currents consisting of low-pass filtered (120-Hz cutoff, 8th-order Butterworth filter) Gaussian white noise with mean relative to the baseline holding current (0.25 nA) and standard deviation (0.2 nA) were applied following previously established techniques (Ellis et al. 2007a,b; Oswald et al. 2004). Cells typically displayed firing rates of 10–25 spikes/s during this stimulation, which is within the range of firing rates observed in vivo under baseline activity (Krahe et al. 2008). Spike times were obtained by thresholding the membrane potential (i.e., spike times were obtained as the times at which the membrane potential crosses a suitably chosen threshold from below). Typical threshold values used were −35 mV. The stimulus waveform S(t) was resampled at 2 kHz, and a binary sequence $X(t)$ also sampled at 2 kHz was then constructed from the spike times. Specifically, time was discretized into binwidths of 0.5 ms. The content of any given bin was set to 1 if an action potential occurred during that bin and to 0 otherwise. Note that because the binwidth is less than the absolute refractory period of ELL pyramidal cells (typically 1–2 ms), there can be at most one action potential occurring during any given bin.

Information theory was developed in the context of communication systems (Shannon 1948) and relies on a numerical quantity termed mutual information. The mutual information quantifies the ability of a system to correctly discriminate between multiple stimuli and is typically expressed in bits: a value of X bits implies that the system can correctly discriminate between 2^X stimuli. The mutual information rate is defined as the mutual information per unit time. In the context of neural systems, investigators are typically interested in applying information theory to quantify the ability of neural populations to discriminate between different stimuli (Borst and Theunissen 1999). One important issue that one is faced with when computing mutual information is that it is in practice impossible to record neural responses to every possible stimulus, and it is thus necessary to make approximations (Chacron et al. 2003). A particularly attractive approximation is to use Gaussian noise stimuli, since the mutual information rate can then be computed from only one presentation of the stimulus (Rieke et al. 1996). Moreover, because sensory stimuli are frequently characterized by their temporal frequency content, it is more informative to look at the mutual information rate density (i.e., the mutual information rate per frequency) rather than the mutual information rate itself. Previous studies have shown that a lower bound on the mutual information rate density I(f) between the stimulus S(t) and the binary sequence $X(t)$ is given by (Borst and Theunissen 1999; Rieke et al. 1996)

$$\mathrm{I}(f) = -\log_2\left[1 - \mathrm{C}(f)\right]$$

and is expressed in bits per second per Hz, where C(f) is the coherence function at temporal frequency f, which is defined as

$$\mathrm{C}(f) = \frac{\left|\mathrm{P_{rs}}(f)\right|^2}{\mathrm{P_{rr}}(f)\mathrm{P_{ss}}(f)}$$

where $\mathrm{P_{rs}}(f)$ denotes the cross spectrum between S(t) and $X(t)$, $\mathrm{P_{ss}}(f)$ is the power spectrum of the stimulus S(t), and $\mathrm{P_{rr}}(f)$ is the power spectrum of the binary sequence $X(t)$. To account for the fact that the mutual information rate density increases with firing rate (Borst and Haag 2001), we normalized it by the mean firing rate, f_r (measured in spikes/s), during stimulation. Thus we computed $\mathrm{MI}(f) = \mathrm{I}(f)/f_r$, where MI($f$) is the normalized mutual information rate density and is measured in bits per spike per Hz. We note that the mutual information rate density I(f) can also be obtained by computing the signal power-to-noise power ratio (SNR) at frequency f and that higher values of the SNR will lead to larger information rates (Borst and Theunissen 1999).

Feature detection analysis. Depending on the behavioral context, it might be more advantageous for a sensory system to detect the presence of particular features present in the sensory environment while ignoring detailed attributes of these features that might be irrelevant to behavioral outcomes. In such a situation, the mutual information would be expected to be low, since the goal is not to distinguish between different stimuli present in the sensory environment but merely to detect their presence. One proposed function for burst firing is precisely to detect such features (Gabbiani 1996; Metzner et al. 1998; Oswald et al. 2004; Sherman 2001; Sherman and Guillary 2002).

We therefore quantified feature detection using a previously described technique (Gabbiani et al. 1996; Metzner et al. 1998; Oswald et al. 2004, 2007). For each bin of the binary sequence $X(t)$, we accumulated a stimulus vector that consisted of the stimulus waveform that preceded the bin over the time range $(t - \Delta t; t)$, where Δt = 100 ms. We then separated these waveforms on whether an event occurred at time t or not. Specifically, we introduced a variable λ that took the value 1 if an event occurred or 0 otherwise (Metzner et al. 1998). We then looked at the resulting waveform distributions conditioned on whether an event occurred, $P(s/\lambda = 1)$, or not, $P(s/\lambda = 0)$. We let m_0 and m_1 be the means of the distributions $P(s/\lambda = 0)$ and $P(s/\lambda = 1)$, respectively. We let Σ_0 and Σ_1 be the covariances of the distributions $P(s/\lambda = 0)$ and $P(s/\lambda = 1)$, respectively. Fisher's linear discriminant function (f^T) was used to determine the optimal feature vector $\mathbf{f}$ that maximizes the SNR.

$$\frac{1}{2}\left(\Sigma_0 + \Sigma_1\right) \cdot f = m_1 - m_0$$

$$\mathrm{SNR} = \frac{\left[f^{T} \cdot \left(m_1 - m_0\right)\right]^2}{f^{T} \cdot \left(\frac{1}{2}\Sigma_0 + \frac{1}{2}\Sigma_1\right) \cdot f}$$

Downloaded from jn.physiology.org on March 25, 2011

The SNR measures the separation between classes normalized by the variance within each class and is thus a measure of discriminability. We used standard bootstrap analysis to estimate the error on the feature vector $\mathbf{f}$ (Davison and Hinkley 2006). The probability of correct detection, P_D (i.e., correctly classifying a stimulus vector as eliciting or not eliciting a spike) and the probability of false alarm, P_{FA} (i.e., misclassifying a stimulus vector as eliciting or not eliciting a spike) can then be determined from the separation between the distributions $P(\mathbf{f}^T \cdot s/\lambda = 1)$ and $P(\mathbf{f}^T \cdot s/\lambda = 0)$. The receiver operating characteristic (ROC) curve (P_D vs. P_{FA}) was plotted for each case. We considered three different events: all spikes, burst events (i.e., the first spike within a burst), and isolated spikes, and computed the separation between the distributions $P(\mathbf{f}^T \cdot s/\lambda = 1)$ and $P(\mathbf{f}^T \cdot s/\lambda = 0)$ in all three cases. We quantified the degree of separation between these distributions by computing the SNR as well as the d′ measure, which is defined by (Green and Swets 1966) as

$$d' = \frac{|\mu_1 - \mu_0|}{\sqrt{\frac{\sigma_1^2 + \sigma_0^2}{2}}}$$

Classification of Pyramidal Cell Type

E- and I-type pyramidal cells within the lateral segment were identified on the basis of their responses to noise current injections, because previous studies have determined that they display differential tuning to such stimuli. Specifically, I-cells display predominantly low-pass responses, whereas E-cells display more broadband responses (Ellis et al. 2007b; Mehaffey et al. 2008a). We defined a selectivity index based on the ratio of the average coherence value between 10 and 50 Hz to the average value between 80 and 120 Hz. We observed that the distribution of selectivity indexes was clearly bimodal (data not shown), and a threshold value of 2 was found to be adequate in separating both modes. The cells whose selectivity indexes were above this threshold (i.e., those that were most low pass) were classified as I-type, whereas the remaining cells were classified as E-type.

Statistical Analysis

Statistical significances were assessed using a Student's *t*-test or a Wilcoxon signed-rank test. All values are means ± SE.

RESULTS

Histology

An earlier study has already described the overall distribution of 5-HT somata and fibers within the brain of *A. leptorhynchus* (Johnston et al. 1990). This report briefly suggested a differential distribution of 5-HT fibers across the maps of the ELL. Given the far greater understanding of the different functions of the three tuberous maps of the ELL (Maler 2009a,b; Marsat et al. 2009; Metzner and Juranek 1997), we used more sensitive immunohistochemical methods (Smith et al. 2006) to reexamine the distribution of 5-HT within the ELL and associated structures and determine whether it might correlate with the hypothesized functions of the tuberous maps.

A 5-HT-immunoreactive (5-HT-ir) fiber bundle located at the ventromedial edge of the ELL sends fibers dorsally and medially to densely innervate the cellular layers of the nucleus medialis (lateral line region; Maler et al. 1974) and medial map of the ELL (in receipt of input from ampullary electroreceptors; Heiligenberg and Dye 1982) (Fig. 1, *A* and *B*); these projections are not further discussed. A lateral branch of the main 5-HT fiber bundle then projected to the tuberous maps of the ELL (Fig. 1, *A* and *B*), where it terminates densely in the lateral segment (LS) with far less staining visible in the centromedial (CMS) and centrolateral (CLS) segments. 5-HTir fibers terminated diffusely and, unlike GABAergic boutons (Maler and Mugnaini 1994), did not appear to surround neuronal somata; this result suggests that 5-HT is likely to have a modulatory role in electrosensory processing. In the CMS, the immunoreactive fibers were mostly confined to the granule cell layer and clearly avoided the spherical cells (Fig. 1*C*); spherical cells are in receipt of gap junction input from time-coding electroreceptors (T-units) (Maler et al. 1981; Mathieson et al. 1987), and their response is invariant (Heiligenberg 1991). In the LS, dense immunoreactivity was observed in the pyramidal cell layer surrounding pyramidal cells (Fig. 1*D*); this extended into the ventral molecular layer, where the 5-HT fibers were in close proximity to the GABAergic neurons of the ventral molecular layer (Maler 1979; Maler and Mugnaini 1994; Maler et al. 1981; Mehaffey et al. 2005). Immunoreactive axons were seen running through the lateral aspect of the granule cell layer at rostral levels, but these were likely fibers of passage since they were not seen at caudal levels (data not shown). Only a small plexus of 5-HT fibers were clearly associated with the neuropil ventral to the granule cells, and the granule cell layer itself appeared to lack a 5-HT terminal plexus. Although 5-HT fibers were seen in the vicinity of ovoid cells (Maler 1979; Middleton et al. 2006), we could not ascertain whether they were fibers of passage or terminated in the vicinity of these interneurons. We can therefore conclude that 5-HT will directly modulate sensory processing by projection (pyramidal) cells of the LS but will have only indirect effects (via inhibitory granular interneurons) in the CMS. We note that weaker direct and indirect modulatory regulation of CLS processing is expected from our immunohistochemical results.

The 5-HT fibers that innervated the ELL continued laterally to form a plexus within the granular layer of the caudal cerebellum (eminentia granularis posterior, EGp); no immunoreactivity was seen in the cerebellar molecular layer. The EGp conveys indirect feedback to the ELL. This 5-HT innervation was precisely confined to the electrosensory portion of the cerebellum, with the rest of the cerebellar granular layer nearly completely devoid of labeling (Fig. 1*A*). The boundary between 5-HT-positive and -negative regions precisely matched the previously established boundary between EGp and corpus cerebellum (Maler et al. 1991; Sas and Maler 1991). Therefore, 5-HT is likely to modulate electrosensory processing in ELL via modulation of its feedback input (see DISCUSSION).

5-HT Application Induces Burst Firing in CLS and LS but Not CMS Neurons

We recorded intracellularly from 96 pyramidal neurons in vitro from the three tuberous ELL segments. These consist of the CMS, CLS, and LS (Fig. 2*A*) and can be easily identified during in vitro recordings (Maler et al. 1991; Mathieson and Maler 1988). There are two pyramidal cell types within each ELL segment. Basilar or E-type pyramidal cells are excited, whereas nonbasilar or I-type cells are inhibited, by increases in stimulus amplitude (Maler 1979; Saunders and Bastian 1984); these cell types correspond to the on and off center cells seen in the retina and lateral geniculate nucleus (Maler et al. 1981).

Downloaded from jn.physiology.org on March 25, 2011

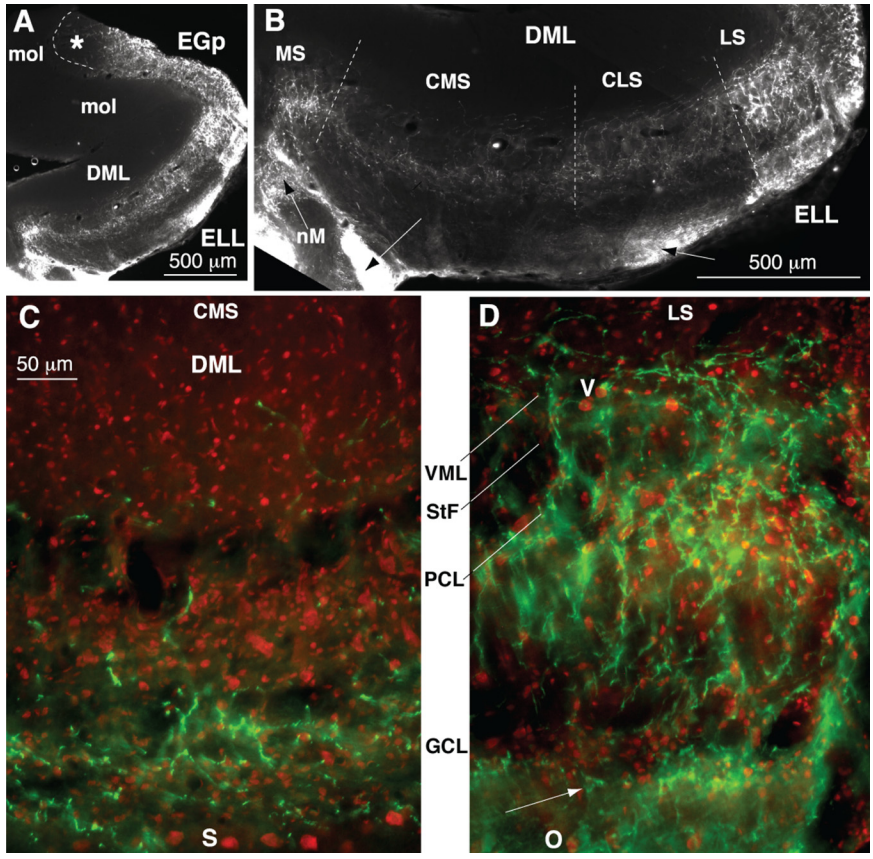

Fig. 1. *A* and *B*: serotonin (5-HT) immunoreactivity in electrosensory lateral line lobe (ELL) and eminentia granularis posterior (EGp). *A*: a patchy distribution of 5-HT immunoreactivity is shown within the cellular layers of the ELL and in the cerebellar region (EGp) that gives rise to feedback to the ELL. There are no 5-HT fibers in the granular layer of the adjacent corpus cerebellum; asterisk is located in the transitional zone of the cerebellum, which neither receives electrosensory feedback input nor projects back to the ELL (Sas and Maler 1987). 5-HT immunoreactivity is also minimal in the molecular layer of the cerebellum (mol) and the analogous dorsal molecular layer of the ELL (DML). *B*: in the same section as *A*, 5-HT fibers in the dorsal medulla enter the ELL and run laterally in its deep fiber layer toward the EGp (unlabeled arrows); medially directed fibers terminate in the lateral line recipient region (nucleus medialis, nM; arrow). Within the ELL, dense 5-HT-immunoreactive plexuses are shown in cellular laminae of the medial (MS) and lateral segments (LS) with lesser amounts in the centromedial (CMS) and centrolateral segments (CLS) (segmental boundaries are indicated by dashed lines). There is minimal immunoreactivity within the DML. *C* and *D*: double label for 5-HT (green) and a fluorescent Nissl stain (red). *C*: 5-HT immunoreactivity in the CMS is mostly confined to the granule cell layer (GCL) with a few 5-HT fibers visible in the pyramidal cell layer (PCL). Note the lack of 5-HT-immunoreactive fibers in the vicinity of the spherical cells (S). *D*: dense 5-HT immunoreactivity is visible in the PCL and the ventral molecular layer (VML) in LS, where it is associated with the neurons of the ventral molecular layer (V). The GCL is mostly free of 5-HT-immunoreactive fibers; those visible at the lateral aspect appear to be mostly fibers of passage, since they are not seen at more caudal levels of the ELL. The arrow points to a 5-HT-positive fiber plexus ventral to the GCL that is visible throughout the LS. 5-HT fibers are also seen in close proximity to ovoid cells (O), although we could not ascertain whether these were merely fibers of passage. StF, stratum tractus fibrosum.

We first compared ELL pyramidal neuron spiking activity under control conditions, after 5-HT application, and after washout. 5-HT application significantly affected the spiking activity of LS neurons (compare Fig. 2, *B* and *C*) in that it caused an increased tendency to fire clusters of action potentials (i.e., bursts). This effect was reversible (compare Fig. 2, *B* and *D*). A similar but albeit weaker effect was observed in CLS neurons (compare Fig. 2, *E* and *F*), and this effect was also reversible (compare Fig. 2, *F* and *G*). In contrast, 5-HT application did not noticeably affect the spiking activity of CMS neurons (compare Fig. 2, *H*, *I*, and *G*).

We next quantified the effects of 5-HT application on the spiking activity by computing the mean firing rate and the ISI distribution. The ISI distributions were similar across all three segments (compare Fig. 3, *A–C*) as previously observed (Mehaffey et al. 2008b). Although 5-HT application did not affect the ISI distribution of CMS neurons (Fig. 3*A*), the ISI distributions of both CLS (Fig. 3*B*) and LS neurons (Fig. 3*C*) were shifted to the left with respect to those obtained under control conditions. We quantified this shift by computing the mean ISI values across our data set and found that the mean ISI under control conditions and after 5-HT application were not significantly different for CMS neurons (control: 45.8 ± 17.8 ms; 5-HT: 38.4 ± 7.9 ms; paired *t*-test, $P = 0.6$, $n = 5$) and were significantly different for both CLS (control: 49.2 ± 13.5 ms; 5-HT: 20.7 ± 10.9 ms; paired *t*-test, $P = 0.03$, $n = 6$) and LS neurons (control: 59.9 ± 20.8 ms; 5-HT: 26.04 ± 14.3 ms; paired *t*-test, $P = 0.03$, $n = 7$). The mean ISI values after 5-HT washout were not significantly different from those obtained under control conditions across all three segments (paired *t*-tests, $P > 0.1$).

We note that the distribution of the logarithm of the ISIs (Turner et al. 1996) computed after 5-HT application was bimodal in nature for LS and CLS neurons but not for CMS neurons (Fig. 3, *A–C*, *insets*). We note that this bimodal nature is often taken to be characteristic of burst firing (Turner et al. 1996; Mehaffey et al. 2008c). We further characterized burst firing by computing the ISI return map (i.e., plotting the value

Downloaded from jn.physiology.org on March 25, 2011

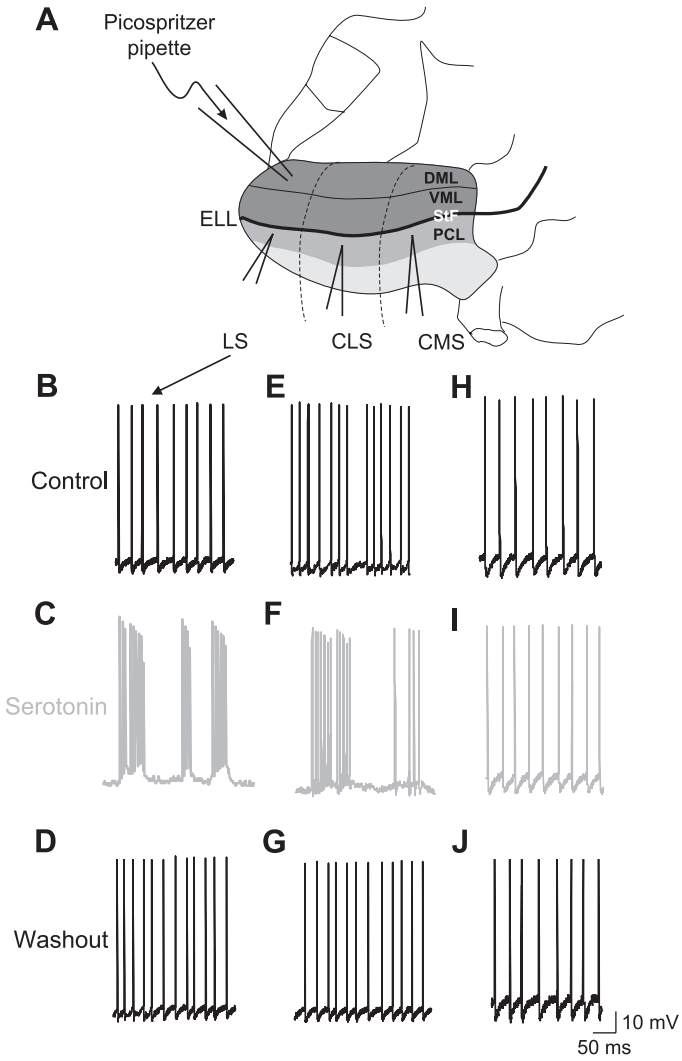

Fig. 2. Effects of 5-HT application are map specific. *A*: schematic of a slice of the hindbrain showing the 3 tuberous segments within the ELL consisting of the CMS, CLS, and LS. The sharp intracellular recording electrode was placed within the PCL within each segment just below the StF. A patch pipette connected to a Picospritzer was placed within the DML, which is just above the VML, and was used to focally apply 5-HT or other drugs, which then diffused to the VML and PCL. *B*: spiking activity recorded under control conditions from an example LS pyramidal neuron. *C*: spiking activity from the same neuron as in *B* after 5-HT application displays burst firing. *D*: spiking activity from the same neuron after 5-HT washout was comparable to that obtained under control conditions. *E*: spiking activity recorded under control conditions from an example CLS pyramidal neuron. *F*: spiking activity from the same neuron as in *E* after 5-HT application displays an increased tendency to display burst firing. *G*: spiking activity from the same neuron after 5-HT washout was comparable to that obtained under control conditions. *H*: spiking activity recorded under control conditions from an example CMS pyramidal neuron. *I*: spiking activity from the same neuron as in *H* after 5-HT application was similar to that obtained under control conditions. *J*: spiking activity from the same neuron after 5-HT washout was comparable to that obtained under control conditions.

of the current ISI as a function of the value of the preceding ISI). An ISI return map that consists of a cluster of points near the identity line is indicative of tonic firing, whereas one that displays an L-shaped cluster along the $x = 0$ and $y = 0$ axes is indicative of burst firing (Ellis et al. 2007b; Mathieson and Maler 1988; Toporikova and Chacron 2009). Our results show that the ISI return maps under control conditions were similar across the three segments and were indicative of tonic firing (compare Fig. 3, *D–F*). Whereas 5-HT application did not have any noticeable effect on the ISI return map of CMS neurons (Fig. 3*D*), it caused those of both CLS (Fig. 3*E*) and LS neurons (Fig. 3*F*) to morph into an L-shaped form that is indicative of burst firing. The effect was most pronounced in LS neurons (Fig. 3*F*). This effect was reversible in both LS and CLS neurons, because after washout, the ISI return maps across all three segments were similar to those obtained under control conditions (Fig. 3, *D–F*).

We next quantified these effects across our data set. Since we found that 5-HT application affected the firing activities of both E- and I-type cells in a quantitatively similar fashion, the data were pooled. 5-HT application caused a significant increase in the mean firing rate of both CLS (control: 43.8 ± 11.0 Hz; 5-HT: 71.9 ± 18.7 Hz; paired *t*-test, $P = 0.03$, $n = 6$) and LS neurons (control 28.5 ± 4.9 Hz; 5-HT 108.8 ± 8.7 Hz; paired *t*-test, $P = 0.01$, $n = 6$) but did not significantly affect the mean firing rate of CMS neurons (control: 29.6 ± 7.3 Hz; 5-HT: 32.3 ± 8.7 Hz; paired *t*-test, $P = 0.7$, $n = 5$) (Fig. 3*G*). The mean firing rate values after washout were not significantly different from those obtained under control conditions ($P > 0.25$ in all cases, paired *t*-tests) across all three segments. 5-HT application significantly increased the burst fraction (i.e., the fraction of ISIs that are <10 ms) of both CLS (control: 0.13 ± 0.09; 5-HT: 0.36 ± 0.11; Wilcoxon signed-rank test, $P = 0.03$, $n = 6$) and LS neurons (control: 0.08 ± 0.01; 5-HT: 0.41 ± 0.03; Wilcoxon signed-rank test, $P = 0.03$, $n = 6$) and did not have a significant effect on the burst fraction of CMS neurons (control: 0.07 ± 0.10; 5-HT: 0.08 ± 0.1; Wilcoxon signed-rank test, $P = 0.06$, $n = 5$). The burst fraction values after washout were not significantly different from those obtained under control conditions ($P > 0.4$ in all cases, Wilcoxon signed-rank tests) across all three segments. Finally, 5-HT application significantly increased the CV of both CLS (control: 0.90 ± 0.09; 5-HT: 1.28 ± 0.10; Wilcoxon signed-rank test, $P = 0.03$, $n = 6$) and LS neurons (control: 0.60 ± 0.10; 5-HT: 1.50 ± 0.10; Wilcoxon signed-rank test, $P = 0.03$, $n = 6$) and did not have a significant effect on the CV of CMS neurons (control: 0.77 ± 0.20; 5-HT: 0.39 ± 0.06; Wilcoxon signed-rank test, $P = 0.1$, $n = 5$). The CV values obtained after washout were not significantly different than those obtained under control conditions ($P > 0.1$ in all cases, Wilcoxon signed-rank tests) across all three segments.

5-HT Reduces the AHP in Pyramidal Neurons

We next turned our attention toward the mechanism by which 5-HT alters the spiking activity of ELL pyramidal cells. A closer inspection of our data revealed that the AHP following each action potential was reduced in the example CLS and LS neurons but not in the CMS neuron (Fig. 2). This was confirmed by plotting the average action potential waveforms under control conditions and after 5-HT application for example CMS and LS neurons (Fig. 4*A*). Although the waveforms almost completely overlapped for the CMS neuron, the AHP was reduced after 5-HT application for the LS neuron.

Previous studies have shown that the AHP can be mediated by different membrane conductances (Faber and Sah 2002; Sah 1996). In particular, large-conductance calcium-activated potassium channels mediate the fast component (Brenner et al. 2005; Matthews et al. 2008), whereas small-conductance (SK)

Downloaded from jn.physiology.org on March 25, 2011

calcium-activated potassium channels and subthreshold voltage-gated M-type potassium channels mediate the medium component of the AHP (mAHP) (Faber and Sah 2002; Sah 1996). On the other hand, various mechanisms have been proposed to mediate the slow component of the AHP; these include alteration in persistent sodium current, M current, and intracellular calcium (Koyama and Appel 2006; Pineda et al. 1999; Schwindt et al. 1989).

We therefore quantified the change in AHP caused by 5-HT application across our population of neurons at different time scales. In particular, our results show that the mAHP (measured at 10–40 ms after the action potential peak) was significantly reduced in both CLS (59.85 ± 9.34%; paired *t*-test, $P = 0.02$, $n = 6$) and LS neurons (22.41 ± 10.62%; paired *t*-test, $P = 0.008$, $n = 13$) but was not altered in CMS neurons (97.32 ± 9.4%; paired *t*-test, $P = 0.4$, $n = 5$) (Fig. 4*B*). In contrast, both the fast (measured at 5 ms after the action potential peak) and slow (measured at 2 s after the AHP) components of the AHP were not altered by 5-HT application in CMS, CLS, or LS neurons (data not shown; $P > 0.4$ in all cases, paired *t*-tests).

These results show that the effects on ELL pyramidal cell activity induced by 5-HT application were consistent in their magnitude with the distribution of 5-HT across the ELL segments. Moreover, the effects of 5-HT application were not qualitatively different in both CLS and LS neurons; we merely observed an overall stronger effect in LS neurons. This suggests a unique mode of action by which 5-HT alters pyramidal neuron excitability and responses to sensory input. We therefore restricted our recordings to LS pyramidal cells, which displayed the greatest changes in excitability contingent on 5-HT application.

Inhibition of SK-Mediated Currents Induced by 5-HT is Specific to E-Cells

The mAHP is often mediated by SK channels (Sah 1996), and previous studies have shown that SK channel antagonists will lead to increased burst firing in E-type ELL pyramidal neurons within CLS and LS through a reduction in the mAHP (Ellis et al. 2007b). Furthermore, a comparison between the distribution of SK channels across the ELL segments (Ellis et al. 2007b, 2008) and our results on the distribution of 5-HT reveals a strong positive correlation between 5-HT and SK channel expression. Indeed, there is a graded level of expression of SK channels across the segments with LS showing the strongest expression and CMS the weakest (Ellis et al. 2007b, 2008). This suggests that 5-HT application decreases the mAHP by inhibiting SK channel-mediated currents.

We therefore performed the following occlusion experiment with the SK channel antagonist UCL-1684 (UCL) and 5-HT on LS pyramidal neurons. We first applied UCL and followed this with 5-HT application. If 5-HT did not have a further effect, then we could say that UCL occluded the effect of 5-HT. We also tested whether 5-HT occluded the effect of UCL by first applying 5-HT and then applying UCL. We report below the results obtained with the mean firing rate as well as the burst fraction, but similar results were obtained using the mAHP (data not shown). Our results show that UCL only partially occluded the effects of 5-HT in E-cells in LS neurons (Fig. 5*A*). Both the average firing rate and burst fraction of neurons increased by about 135% (control: 20.1 ± 4.5 spikes/s; UCL: 46.8 ± 6.3 spikes/s; paired *t*-test, $P = 0.002$, $n = 6$) and 550% (control: 0.05 ± 0.01; UCL: 0.3 ± 0.1; paired *t*-test, $P = 0.009$, $n = 6$), respectively, after UCL application. Subsequent 5-HT application, however, led to a further increase in both firing rate (~60%; UCL+5-HT: 73.7 ± 10.1 spikes/s, paired *t*-test, $P = 0.03$, $n = 6$) and burst fraction (~30%; UCL+5-HT: 0.4 ± 0.1; paired *t*-test, $P = 0.04$, $n = 6$). We note that it is unlikely that this result is a consequence of UCL only partially blocking SK channels given the UCL concentrations used in this study. However, the effects of UCL were occluded by prior application of 5-HT, indicating that SK-mediated currents were indeed reduced under 5-HT application (Fig. 5*B*). Indeed, whereas 5-HT application led to a significant increase in both firing rate (~120%; control: 24.56 ± 3.2 spikes/s; 5-HT: 54.6 ± 3.4 spikes/s; paired *t*-test, $P = 0.006$, $n = 6$) and burst fraction (~640%; control: 0.04 ± 0.01; 5-HT: 0.3 ± 0.04; paired *t*-test, $P = 0.17$, $n = 6$), subsequent UCL application did not lead to a further increase in either firing rate (~10%; 5-HT+UCL: 58.7 ± 4.4 spikes/s; paired *t*-test, $P = 0.1$, $n = 6$) or burst fraction (~9%; 5-HT+UCL: 0.33 ± 0.02; paired *t*-test, $P = 0.7$, $n = 6$). We conclude that 5-HT application does lead to a reduction of SK-mediated currents but that this reduction does not account for the full effect of 5-HT in E-cells.

The situation was different in I-cells, because our results show that UCL application did not significantly affect their mean firing rate (control: 22.3 ± 4.2 spikes/s; UCL: 27.5 ± 6.1 spikes/s; paired *t*-test, $P = 0.11$, $n = 6$) or burst fraction (control: 0.05 ± 0.02; UCL: 0.06 ± 0.02; paired *t*-test, $P = 0.17$, $n = 6$). However, subsequent 5-HT application led to a significant increase in firing rate (~80%; UCL+5-HT: 50.4 ± 8.5 spikes/s; paired *t*-test, $P = 0.008$, $n = 6$) as well as burst fraction (~530%; UCL+5-HT: 0.4 ± 0.2; paired *t*-test, $P = 0.04$, $n = 6$) (Fig. 5*C*). The reverse experiment led to the following results: initial 5-HT application led to significant increases in both the mean firing rate (~115%; control: 26.6 ± 3.9 spikes/s; 5-HT: 57.8 ± 7.8 spikes/s; paired *t*-test, $P = 0.01$, $n = 5$) and burst fraction (~360%; control: 0.04 ± 0.01; 5-HT: 0.2 ± 0.1; paired *t*-test, $P = 0.02$, $n = 5$), but subsequent UCL application did not lead to a further change in either mean firing rate (~5%; 5-HT+UCL: 60.7 ± 8.2 spikes/s; paired *t*-test, $P = 0.8$, $n = 5$) or burst fraction (~11%; 5-HT+UCL: 0.22 ± 0.1; paired *t*-test, $P = 0.7$, $n = 5$) (Fig. 5*D*). These results indicate that 5-HT application affects a current other than the one mediated by SK channels in I-cells.

5-HT Application Leads to a Reduction of Subthreshold Potassium Channels in Both E- and I-Cells

We next investigated whether 5-HT application affected subthreshold currents by measuring the subthreshold membrane resistance before and after 5-HT application. 5-HT increased the input resistance of ELL pyramidal neurons in LS (Fig. 6*A*) (from 17.3 ± 2.1 to 33.6 ± 2.9 MΩ, or ~100%). This increase was quantitatively similar in both E- and I-cells and, furthermore, was statistically significant (control vs. 5-HT, Wilcoxon signed-rank test, $P = 0.002$, $n = 10$). One possibility consistent with previous studies is that 5-HT application led to a reduced subthreshold potassium current in both E- and I-cells. M-type potassium currents are known to be activated in the subthreshold region and have been shown to

Downloaded from jn.physiology.org on March 25, 2011

mediate the mAHP in other systems (Gu et al. 2005; Lerche et al. 2000; Shah et al. 2002; Shapiro et al. 2000; Sogaard et al. 2001; Yue and Yaari 2004). We thus hypothesized that 5-HT application inhibits M currents in ELL pyramidal neurons.

We therefore used the selective M current antagonists XE-991 and linopirdine. Our results show that bath application of XE-991 led to a significant change in ELL pyramidal neuron activity and promoted burst firing (Fig. 7*A*) in a manner that is similar to that seen with 5-HT application (compare Figs. 7*A* and 2*C*). Similar results were obtained with linopirdine (Supplemental Fig. 1). (Supplemental data is available online at the *Journal of Neurophysiology* website.)

We therefore performed occlusion experiments similar to the ones described above for SK channels but using M current antagonists instead. Our results show that prior application of XE-991 occluded the effect of 5-HT in I-cells (Fig. 7*B*). Indeed, XE-991 application led to a significant increase in both the mean firing rate (~100%; control: 21.2 ± 1.3 spikes/s; XE-991: 43.4 ± 5.3 spikes/s, paired *t*-test, $P = 0.01$, $n = 8$) and burst fraction (~770%; control: 0.03 ± 0.001; XE-991: 0.26 ± 0.03 paired *t*-test, $P = 0.03$, $n = 8$). However, subsequent 5-HT application did not lead to any further significant change in either firing rate (~20%; XE-991+5-HT: 52.4 ± 12.6 spikes/s; paired *t*-test, $P = 0.9$, $n = 8$) or burst fraction (~2%; XE-991+5-HT: 0.27 ± 0.09; paired *t*-test, $P = 0.9$, $n = 8$). These results show that the mechanism of action of 5-HT in I-cells is through the reduction of an M-type potassium current.

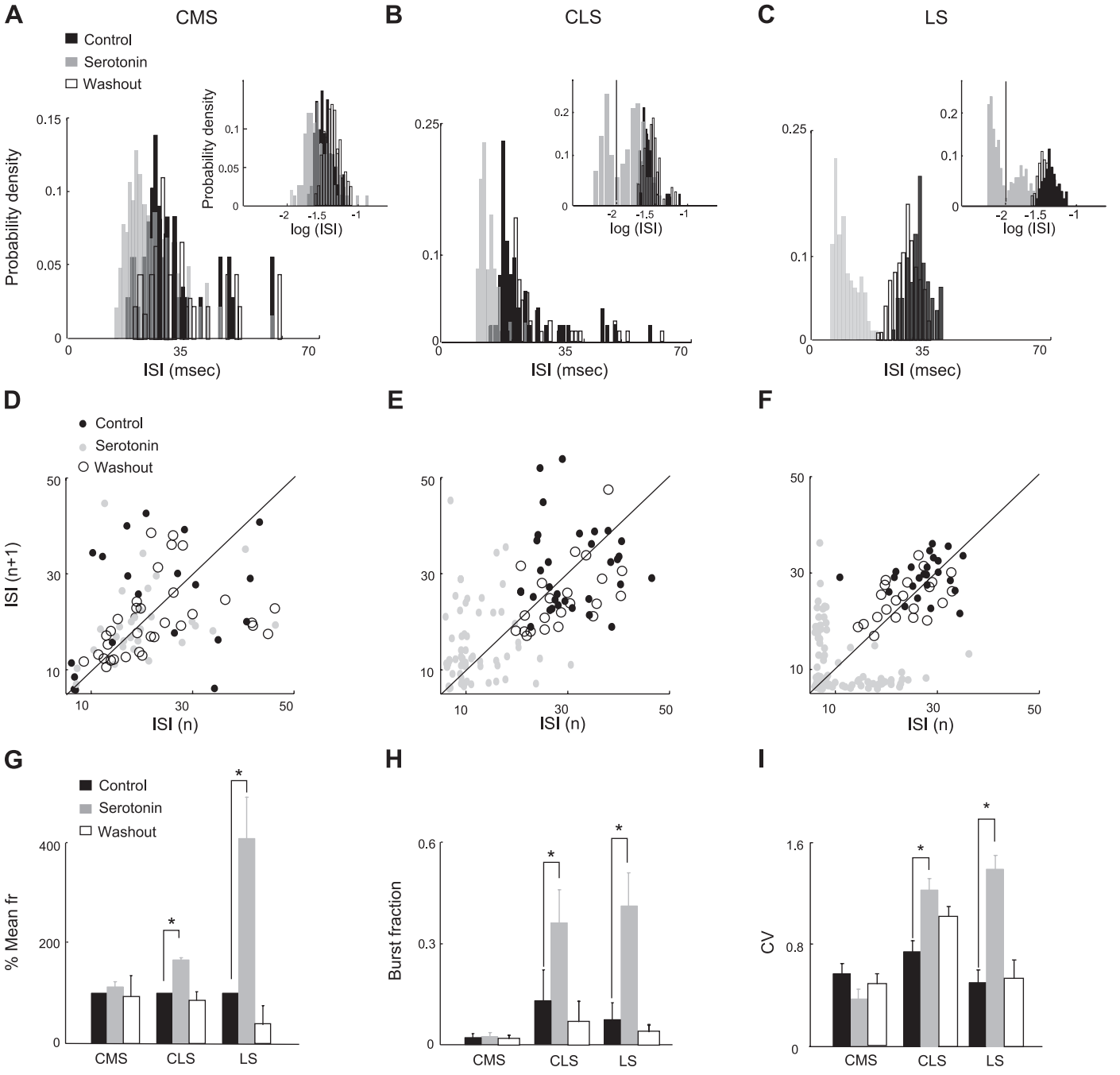

Downloaded from jn.physiology.org on March 25, 2011

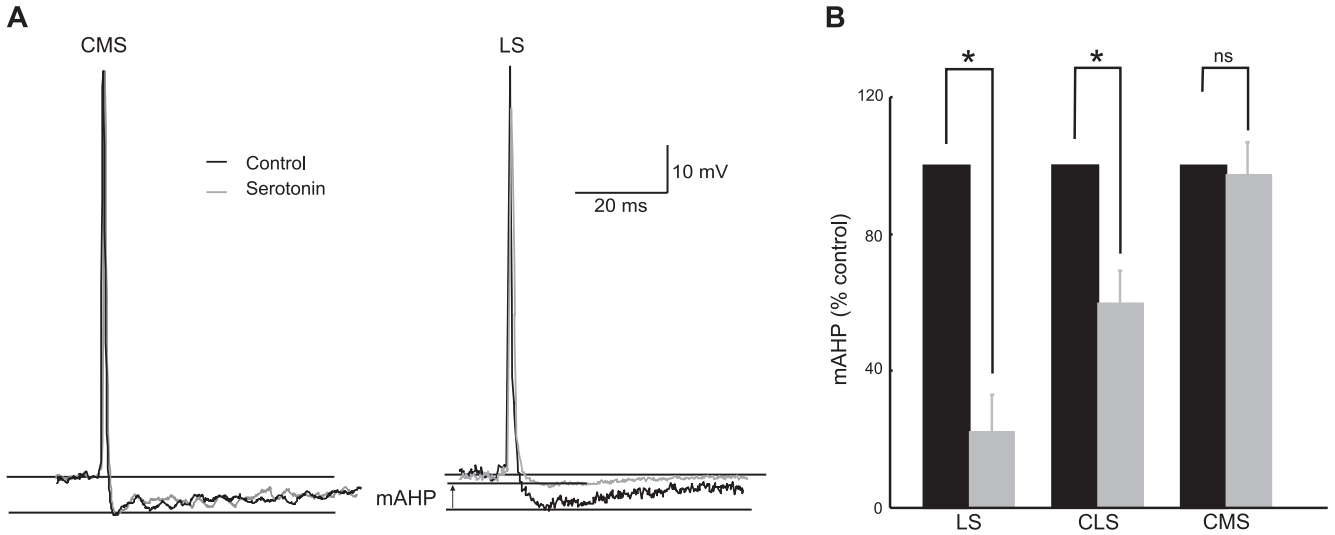

Fig. 4. 5-HT increases pyramidal neuron excitability through a reduction of the afterhyperpolarization (AHP). *A*: average action potential waveforms from example CMS and LS pyramidal neurons under control conditions and after 5-HT application. Whereas there was almost complete overlap between the 2 curves for the CMS neuron, there was a reduction in the AHP following the action potential for the LS neuron. *B*: 5-HT application led to significant reduction in the medium component of the AHP (mAHP) in LS and CLS but not in CMS pyramidal neurons. Asterisks indicate statistical significance at the $P = 0.05$ level using a paired *t*-test; ns, not significant.

Furthermore, our results show that XE-991 also led to a significant increase in the firing rate (~110%; control: 32.3 ± 9.0 spikes/s; XE-991: 67.2 ± 10.6 spikes/s; paired *t*-test, $P = 0.004$, $n = 6$) and burst fraction (~470%; control: 0.04 ± 0.001; XE-991: 0.23 ± 0.04; paired *t*-test, $P = 0.009$, $n = 6$) of E-cells (Fig. 7*C*). Subsequent 5-HT application led to further significant increases in both firing rate (~20%; XE-991+5-HT: 79.8 ± 12.9 spikes/s; paired *t*-test, $P = 0.03$, $n = 6$) and burst fraction (~30%; XE-991+5-HT: 0.29 ± 0.07; paired *t*-test, $P = 0.04$, $n = 6$). We hypothesized that 5-HT application leads to reduced SK and M currents in E-cells. As such, the subsequent increase in firing rate seen when 5-HT was applied after XE-991 should be due to reduced SK channel-mediated currents. To test this hypothesis, we performed the following experiment: initial XE-991 application, followed by UCL application and, finally, by 5-HT application.

Our results show that XE-991 application to E-cells led to a significant increase in the mean firing rate (~115%; control: 20.3 ± 7.7 spikes/s; XE-991: 43.04 ± 9.8 spikes/s; paired *t*-test, $P = 0.002$, $n = 9$) and burst fraction (~370%; control: 0.02 ± 0.08; XE-991: 0.1 ± 0.04; paired *t*-test, $P = 0.005$, $n = 9$). Subsequent UCL application led to further significant increases in both the mean firing rate (~70%; XE-991+UCL: 73.4 ± 8.4 spikes/s; paired *t*-test, $P < 0.001$, $n = 9$) and burst fraction (~30%; XE-991+UCL: 0.14 ± 0.05; paired *t*-test, $P = 0.04$, $n = 9$). However, subsequent 5-HT application did not lead to a further significant change in the mean firing rate (approximately −15%; XE-991+UCL+5-HT: 64.4 ± 6.6 spikes/s; paired *t*-test, $P = 0.7$, $n = 9$) and burst fraction (~14%; XE-991+UCL+5-HT: 0.16 ± 0.09 paired *t*-test, $P = 0.2$, $n = 9$). These results show that 5-HT leads to reduced SK as well as M currents in E-cells. We note that similar results were obtained by quantifying the effects of 5-HT using the mAHP as well as the burst fraction (data not shown). The results obtained using pharmacology are summarized in Table 1.

Fig. 3. 5-HT application induces burst firing in ELL pyramidal neurons. *A*: interspike interval (ISI) probability densities of an example CMS pyramidal neuron obtained under control conditions, after 5-HT application, and after 5-HT washout were similar. *Inset* shows the same ISI distributions but plotted on a logarithmic scale. *B*: ISI probability densities of an example CLS pyramidal neuron obtained under control conditions, after 5-HT application, and after 5-HT washout. Whereas the ISI probability densities under control conditions and after 5-HT application were similar, the ISI probability density after 5-HT application was shifted to the left. *Inset* shows the same ISI distributions but plotted on a logarithmic scale. The ISI distribution under 5-HT application is clearly bimodal, which is characteristic of burst firing. The vertical dashed line shows that the trough between the 2 modes is located at 10 ms. *C*: ISI probability densities of an example LS pyramidal neuron obtained under control conditions, after 5-HT application, and after 5-HT washout. Whereas the ISI probability densities under control conditions and after 5-HT application were similar, the ISI probability density after 5-HT application was shifted to the left. *Inset* shows the same ISI distributions but plotted on a logarithmic scale. The ISI distribution under 5-HT application is clearly bimodal, which is characteristic of burst firing. The vertical dashed line shows that the trough between the 2 modes is located at 10 ms. *D*: ISI return maps of the same example CMS neuron as in *A* under control conditions, after 5-HT application, and after 5-HT washout were similar and consisted of clusters of points around the identity line (dashed), which is indicative of tonic firing. *E*: ISI return maps of the same example CLS neuron as in *B* under control conditions, after 5-HT application, and after 5-HT washout. Whereas the ISI return maps under control conditions and after 5-HT application were similar, the ISI return map after 5-HT application was indicative of burst firing. *F*: ISI return maps of the same example LS neuron as in *C* under control conditions, after 5-HT application, and after 5-HT washout. Whereas the ISI return maps under control conditions and after 5-HT application were similar, the ISI return map after 5-HT application was clearly L-shaped, which is indicative of burst firing. *G*: mean firing rates (f_r) under control conditions, after 5-HT application, and after 5-HT washout. 5-HT application led to a significant increase in the mean firing rate only in the CLS and LS segments that returned to control values after 5-HT washout. *H*: burst fractions under control conditions, after 5-HT application, and after 5-HT washout. 5-HT application led to a significant increase in burst fraction only in the CLS and LS segments that returned to control values after 5-HT washout. *I*: coefficient of variation (CV; defined as the standard deviation-to-mean ratio of the ISI probability density) under control conditions, after 5-HT application, and after 5-HT washout. 5-HT application led to a significant increase in CV only in the CLS and LS segments that returned to control values after 5-HT washout. Asterisk indicates statistical significance at the $P = 0.05$ level using either a paired *t*-test (mean f_r) or a Wilcoxon signed-rank test (burst fraction and CV).

Downloaded from jn.physiology.org on March 25, 2011

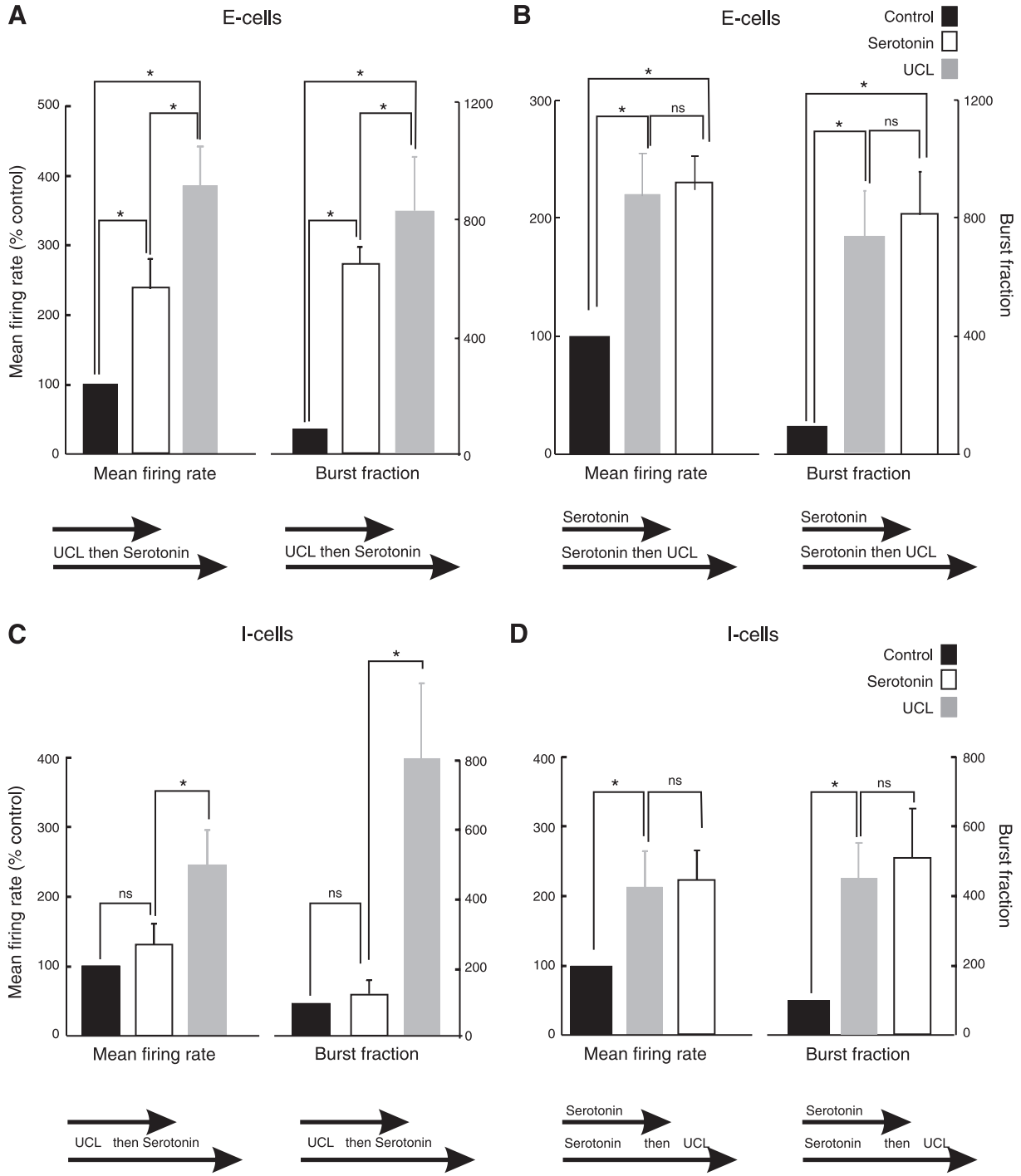

Fig. 5. 5-HT application leads to a reduction of small-conductance calcium-activated (SK) currents in E- but not in I-type LS pyramidal neurons. *A*: mean firing rates (*left*) and mean burst fractions (*right*) of E-type pyramidal neurons under control conditions, after UCL-1684 (UCL; SK channel antagonist) application, and after subsequent 5-HT application. UCL led to significant increases in both firing rate and burst fraction, but subsequent 5-HT application led to further significant increases. As such, UCL application only partially occluded the effects of 5-HT application in E-cells. *B*: mean firing rates (*left*) and mean burst fractions (*right*) of E-type pyramidal neurons under control conditions, after 5-HT application, and after subsequent UCL application. 5-HT led to significant increases in both firing rate and burst fraction, but subsequent UCL application did not lead to any further significant changes in either firing rate or burst fraction. As such, 5-HT application occluded the effects of UCL in E-cells. *C*: mean firing rates (*left*) and mean burst fractions (*right*) of I-type pyramidal neurons under control conditions, after UCL application, and after subsequent 5-HT application. UCL had no significant effect on either mean firing rate or burst fraction, but subsequent 5-HT application led to a significant increase in firing rate as well as burst fraction. As such, UCL application did not occlude the effects of 5-HT. *D*: mean firing rates (*left*) and mean burst fractions (*right*) of I-type pyramidal neurons under control conditions, after 5-HT application, and after subsequent UCL application. 5-HT led to significant increases in firing rate and burst fraction, but subsequent UCL application did not led to any further changes in either firing rate or burst fraction. Asterisks indicate statistical significance at the $P = 0.05$ level using a paired *t*-test.

Downloaded from jn.physiology.org on March 25, 2011

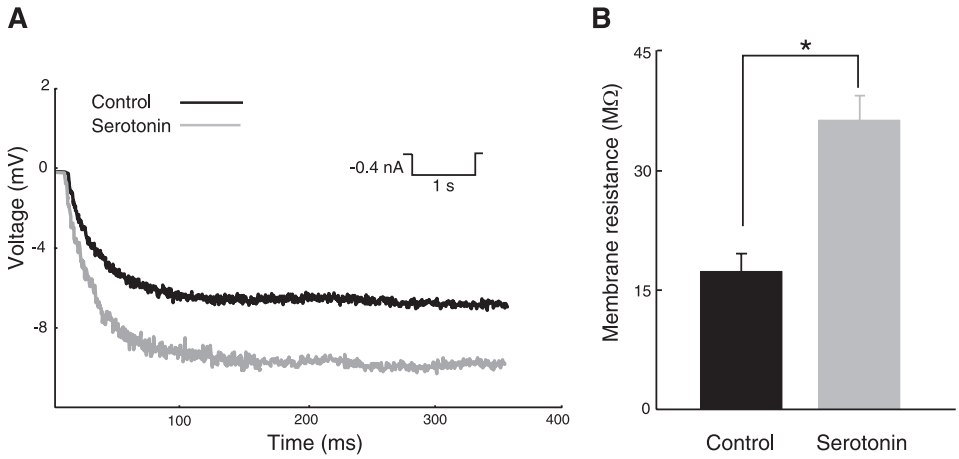

Fig. 6. 5-HT application increases the subthreshold membrane resistance of LS pyramidal neurons. *A*: voltage traces from an example LS neuron under control conditions and after 5-HT application in response to a −0.4 nA current injection. The voltage deflection after 5-HT application was greater, which indicates an increase in the subthreshold membrane resistance. *B*: population averaged subthreshold membrane resistance was significantly larger after 5-HT application. Asterisk indicates statistical significance at the $P = 0.05$ level using a paired *t*-test.

5-HT Application Decreases the First Spike Latency in Both E- and I-Cells

We next investigated the functional role of 5-HT in ELL pyramidal neurons. To address this important question, we first studied the effect of 5-HT application on the spiking activity in response to step current injection. Our results show that both E- and I-type ELL pyramidal neurons within LS tended to respond to such steps with a long latency (~47 ms) and through tonic firing (Fig. 8*A*). In contrast, these same neurons responded to such steps with a burst of action potentials and with a shorter latency (~3 ms) after 5-HT application. The decrease in first spike latency induced by 5-HT application was significant for both E-cells (~58% control vs. 5-HT; paired *t*-test, $P < 0.001$, $n = 12$) (Fig. 8*B*) and I-cells (~55% control vs. 5-HT; paired *t*-test, $P < 0.001$, $n = 6$) (Fig. 8*C*).

5-HT Application Leads to a Decrease in the Current Required to Elicit Action Potential Firing and Increases the Gain of the Response to Constant Stimuli

We next computed the firing rate as a function of the injected current (i.e., the *f-I* curve) before and after 5-HT application. Our results show that 5-HT application resulted in a leftward shift of the *f-I* curve and an increase in its slope in an example E-cell (Fig. 8*D*). We quantified these changes by computing the rheobase current (i.e., the minimum value of the holding current for which spiking activity was observed) and the gain (i.e., the slope of the *f-I* curve). Our results show that 5-HT application did not significantly affect the gain of I-cells (control: 0.12 ± 0.02 spike·ms^{-1}·nA^{-1}; 5-HT: 0.15 ± 0.03 spike·ms^{-1}·nA^{-1}; paired *t*-test, $P = 0.4$, $n = 6$) (Fig. 8*E*) but led to a significant decrease in the rheobase current value (control: −0.1 ± 0.17 nA; 5-HT: −0.7 ± 0.2 nA; paired *t*-test, $P = 0.002$, $n = 6$) (Fig. 8*F*). In E-cells, 5-HT application significantly increased the gain (control: 0.12 ± 0.02 spike·ms^{-1}·nA^{-1}; 5-HT: 0.23 ± 0.04 spike·ms^{-1}·nA^{-1}; paired *t*-test, $P = 0.03$, $n = 6$) (Fig. 8*G*) and significantly decreased the rheobase current (control: −0.05 ± 0.2 nA; 5-HT: −0.3 ± 0.17 nA; paired *t*-test, $P = 0.007$, $n = 6$) (Fig. 8*H*). These results show that 5-HT can significantly alter the threshold current for eliciting action potential firing in both E- and I-cells as well as modulate the gain of E-cells.

5-HT Application Enables Parallel Processing by Different Action Potential Patterns

What are the consequences of the increased tendency for pyramidal cells to display burst firing under 5-HT application on their responses to time-varying sensory input? To determine this, we took advantage of the fact that the tuning of ELL pyramidal neurons to time-varying noise current injections in vitro is similar to that observed in vivo in response to sensory input (Krahe et al. 2008; Mehaffey et al. 2008b) (Fig. 9*A*). We therefore injected noise current waveforms through the recording electrode and measured the spiking response to this input as done previously (Ellis et al. 2007a; Mehaffey et al. 2008b,c; Oswald et al. 2004). We then used information theory (Borst and Theunissen 1999) to quantify the mutual information transmitted by ELL pyramidal neurons about each frequency component of the time-varying noise stimulus. The mutual information measures the ability of a decoder to discriminate between different stimuli using the spiking response (Shannon 1948): X bits of information imply that the system can distinguish between 2^X stimuli (Rieke et al. 1996). Because previous studies have shown that bursts of action potentials produced by ELL pyramidal neurons could code for stimulus features that were distinct from those coded for by isolated spikes, we used an ISI threshold of 10 ms to assign spikes in response to a time-varying noise stimulus as belonging to bursts; spikes that did not belong to bursts were termed isolated spikes (Oswald et al. 2004). This procedure allowed us to separate the spike train into the burst spike train (i.e., the train of spikes that belong to bursts) and the isolated spike train (i.e., the train of spikes that do not belong to bursts). It was then possible to compute the mutual information rate density (i.e., the mutual information rate per frequency) between the burst spike train and the time-varying noise stimulus as well as the mutual information rate density between the isolated spike train and the time-varying noise stimulus (Oswald et al. 2004).

Under control conditions, we rarely observed burst activity, and consequently, the spike train in response to a time-varying noise stimulus consisted almost exclusively of isolated spikes. It is therefore not surprising that the mutual information rate density curve computed from the isolated spike train was almost equal to that computed using all spikes (Fig. 9*B*). The situation was, however, different after 5-HT application, because the spike train now consisted of a mix of burst and

Downloaded from jn.physiology.org on March 25, 2011

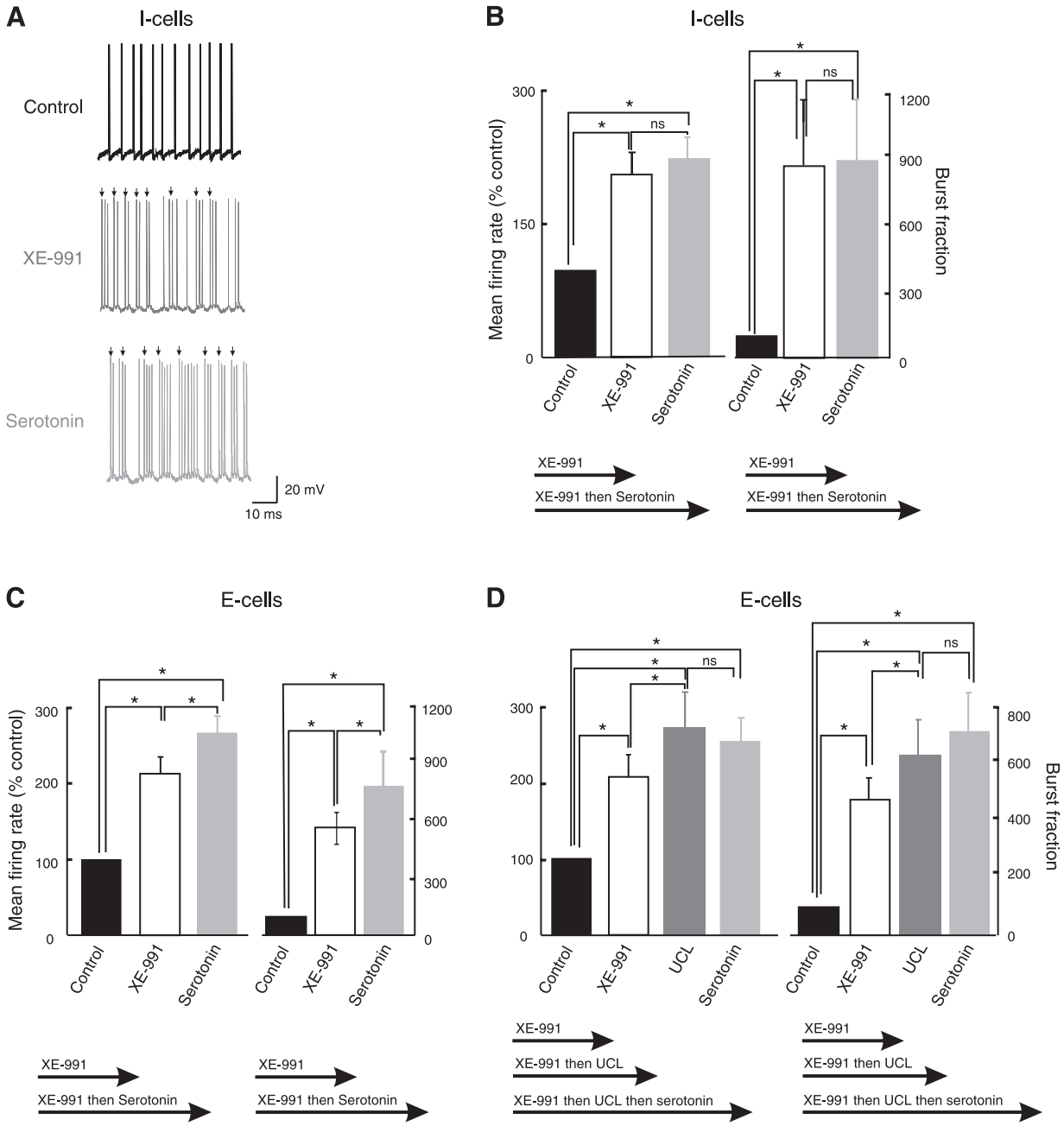

Fig. 7. 5-HT application leads to a reduction of the M current in both E- and I-type LS pyramidal neurons. *A*: spiking activity from an example I-type pyramidal neuron under control conditions (*top*), after application of the selective M current antagonist XE-991 (*middle*), and after subsequent 5-HT application (*bottom*). XE-991 application led to burst firing (arrows) in this particular neuron. Moreover, the spiking activities after XE-991 application and those obtained after subsequent 5-HT application were similar. *B*: mean firing rates (*left*) and mean burst fractions (*right*) of I-type pyramidal neurons under control conditions, after XE-991 application, and after subsequent 5-HT application. XE-991 led to significant increases in both firing rate and burst fraction, but subsequent 5-HT application did not lead to any further significant change in either. As such, XE-991 application occluded the effects of 5-HT application in I-cells. *C*: mean firing rates (*left*) and mean burst fractions (*right*) of E-type pyramidal neurons under control conditions, after XE-991 application, and after subsequent 5-HT application. XE-991 led to significant increases in both firing rate and burst fraction, but subsequent 5-HT did lead to further significant increases in both. As such, XE-991 application only partially occluded the effects of 5-HT application in E-cells. *D*: mean firing rates (*left*) and mean burst fractions (*right*) of E-type pyramidal neurons under control conditions, after XE-991 application, after subsequent UCL application, and after subsequent 5-HT application. XE-991 led to significant increases in both the mean firing rate and the burst fraction. Subsequent UCL application led to further significant increases in both the mean firing rate and the burst fraction. However, subsequent 5-HT application did not lead to any further significant changes in either. This indicates that UCL and XE-991 together could occlude the effects of 5-HT in E-type pyramidal neurons.

isolated spikes. We observed a net decrease in the mutual information rate density when considering all spikes, and this was reflected by a significant decrease in the mutual information rate (i.e., the mutual information rate density integrated over frequency) for both I-cells (control: 1.50 ± 0.14 bits/spike; 5-HT: 1.03 ± 0.13 bits/spike; paired *t*-test, $P = 0.005$, $n = 7$) and E-cells (control: 1.02 ± 0.11 bits/spike; 5-HT: 0.4 ± 0.1 bits/spike; paired *t*-test, $P = 0.009$, $n = 6$).

We next compared the mutual information rate density curves of the burst and isolated spike trains under 5-HT

Downloaded from jn.physiology.org on March 25, 2011

Table 1. *Summary of results on the effects of 5-HT on membrane conductances in E- and I-cells*

Condition	E-Cells	I-Cells
UCL	Partial occlusion of 5-HT	No significant effect
XE-991	Partial occlusion of 5-HT	Complete occlusion of 5-HT
UCL+XE-991	Complete occlusion of 5-HT	Not tested
5-HT	Inhibition of both SK and M currents	Inhibition of M current

UCL, UCL-1684; 5-HT, serotonin; SK, small-conductance calcium-activated potassium current.

application. While the mutual information rate density of isolated spikes was broadband (Fig. 9*C*), the mutual information rate density curve computed from the burst train displayed peaks at both low (~10 Hz) and high (~90 Hz) frequencies (Fig. 9*C*). Our results thus show that the burst and isolated spike trains have qualitatively different mutual information rate density curves under 5-HT application. We quantified these changes by computing a selectivity index that was defined as the ratio between the average mutual information rate density at low frequencies (10–50 Hz) to that at high frequencies (80–120 Hz). As such, a uniform response would have a selectivity index of 1; values greater or smaller than unity imply that the mutual information rate density at low temporal frequencies is greater or smaller than that at high temporal frequencies. Our results show that although 5-HT application did not significantly alter the selectivity index of the isolated spikes (control: 1.80 ± 0.15 bits/spike; 5-HT: 1.30 ± 0.18 bits/spike; paired *t*-test, $P = 0.35$, $n = 8$) (Fig. 9*D*), it led to a significant increase in the selectivity index of the burst spikes (control: 0.36 ± 0.20 bits/spike; 5-HT: 3.20 ± 0.50 bits/spike; paired *t*-test, $P = 0.008$, $n = 8$) (Fig. 9*D*). Furthermore, we observed that isolated spikes now displayed a larger mutual information rate at high frequencies (50–90 Hz) than under control conditions for both E-cells (control: 0.020 ± 0.001 bits/spike; 5-HT: 0.030 ± 0.003 bits/spike; paired *t*-test, $P = 0.003$, $n = 8$) and I-cells (control: 0.020 ± 0.002 bits/spike; 5-HT: 0.030 ± 0.004 bits/spike; paired *t*-test, $P = 0.02$, $n = 8$) (Fig. 9*C*, *inset*). These results show that under 5-HT application, different stimulus features elicit bursts and isolated spikes. We note that since burst firing was rarely observed under control conditions, it was not possible for us to explicitly compare the coding of stimulus features by bursts under control conditions and after 5-HT application.

Previous studies have shown that bursts of action potentials induced by 5-HT application are more apt at detecting stimulus features than isolated spikes (Gabbiani et al. 1996; Metzner et al. 1998; Oswald et al. 2004). As such, we used signal detection theory to quantify how reliable different stimulus features were at eliciting bursts, isolated spikes, and all spikes. In practice, we treated the bursts as events by only considering the first spike within each burst, and we henceforth refer to these as burst events. We then quantified the optimal discriminability between the distribution of stimulus waveforms that trigger burst events, isolated spikes, or any spike versus the distribution of stimulus waveforms that do not trigger spikes or bursts (i.e., the null distribution). This was done by first computing the optimal feature vectors that maximize the separation between the distribution of stimulus waveforms that trigger either burst events, isolated spikes, or any spike versus the null distribution. These feature vectors are shown in Fig. 9*E* and are very similar in shape for all spikes and isolated spikes, that is, similar feature vectors separate isolated spikes or any spike from the null vector (stimuli that do not trigger a spike); the burst feature vector is somewhat different, demonstrating that different feature vectors are required to maximally separate burst-triggering versus null events. Second, we projected each individual stimulus waveform onto the appropriate feature vector and computed the distribution of these projections. The projection is computed by taking the inner (dot) product of the two vectors and is a measure of the amount of correlation between them. Specifically, we computed the distributions obtained from burst events, any spike, isolated spikes, and no spikes (i.e., the null distribution). These distributions give us the following information: their mean indicates how similar the average stimulus waveform that triggers each event (i.e., either of no spike, any spike, burst event, or isolated spike) was to its feature vector. In contrast, their variances reflect the variability in the stimulus waveforms that trigger each event. The distributions of these inner products are shown for an example neuron, and they were all different from one another (Fig. 9*F*). Of most importance, however, is the fact that the distribution derived from the burst feature vector was more distinct from the null distribution than that of any spike or isolated spikes, thereby clearly demonstrating the greater discriminability of stimulus waveforms triggering bursts from the null waveforms (Fig. 9*F*). Because the feature vectors were roughly similar in shape for all three cases, these differences largely originate in the stimulus waveforms that trigger burst events, all spikes, or isolated spikes as described previously (Oswald et al. 2004). These differences were furthermore reflected in the ROC curve obtained from burst events, which was closer to that obtained from an optimal detector than that obtained from either isolated spikes or all spikes (Fig. 9*G*). We further quantified the degree to which the distributions obtained from burst events, all spikes, and isolated spikes were separable from the null distribution by computing the d' measure. We obtained $d' = 3.9$ for burst events, 2.2 for all spikes, and 1.9 for isolated spikes for this example. As such, burst events were better feature detectors than isolated spikes or all spikes for this particular neuron. We next quantified the ability of burst events, isolated spikes, and all spikes to detect their respective optimal features by computing the SNR across our data set. Our results show that SNR computed from burst events was significantly higher than SNR computed from isolated spikes (burst spikes: 8.6 ± 2.1; isolated spikes: 5.5 ± 0.9; Wilcoxon signed-rank test, $P < 0.001$, $n = 15$) or all spikes (burst spikes: 8.6 ± 2.1; all spikes: 5.4 ± 1; Wilcoxon signed-rank test, $P < 0.001$, $n = 15$) (Fig. 9*G*, *inset*).

As such, our results show that after 5-HT application, burst events are better feature detectors than isolated spikes or all spikes. Furthermore, the stimulus features that trigger burst firing are different from those that trigger isolated spikes (Fig. 9*C*). Together with the fact that 5-HT application leads to shorter first spike latencies and decreases the current threshold required to elicit action potential firing, this suggests that the function of the 5-HT system in the ELL is to make pyramidal neurons of the LS map more apt at detecting features present in the sensory environment through burst firing while at the same time making them better estimators of high-frequency stimuli through isolated spike firing. The implications of these results

Downloaded from jn.physiology.org on March 25, 2011

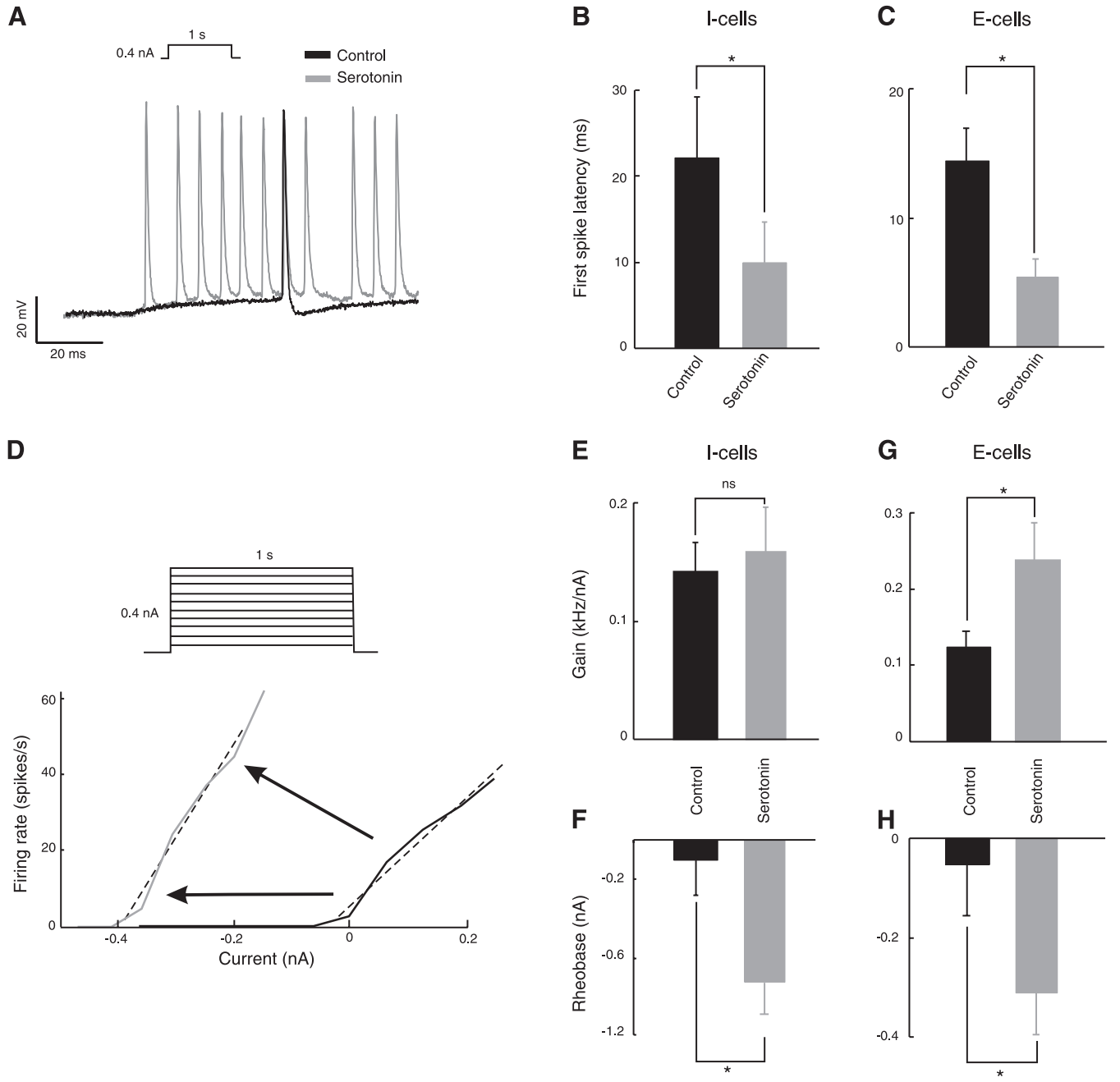

Fig. 8. 5-HT application alters pyramidal neuron responses to current steps. *A*: voltage response from a typical I-type LS pyramidal neuron under control conditions and after 5-HT application in response to a 0.4 nA current step. *B*: the first spike latency (i.e., the time interval between the onset of the step and the first spiking time) was significantly reduced after 5-HT application in I-cells. *C*: the first spike latency was also significantly reduced after 5-HT application in E-cells. *D*: frequency-current (*f-I*) curve showing the mean firing rate as a function of the holding current for a typical E-type LS pyramidal neuron under control conditions (solid curve) and after 5-HT application (shaded curve). 5-HT application increased the slope of the *f-I* curve as determined from a linear fit (dashed lines) and furthermore decreased the minimum amount of current needed to elicit spiking activity (i.e., the rheobase current). *E*: 5-HT application did not significantly alter the gain for I-type pyramidal neurons. *F*: 5-HT application significantly reduced the rheobase current in I-type pyramidal neurons. *G*: 5-HT application led to a significant increase in gain for E-type pyramidal neurons. *H*: 5-HT application significantly reduced the rheobase current in E-type pyramidal neurons. Asterisks indicate statistical significance at the $P = 0.05$ level using a paired *t*-test.

for the processing of sensory stimuli in weakly electric fish and in other systems are discussed at length below.

DISCUSSION

Summary of Results

We investigated the distribution and function of ELL serotonergic inputs. First, we showed that 5-HT displayed a striking differential distribution across the ELL segments, with CMS showing the least and LS showing the most expression. 5-HT application led to increased excitability and promoted burst firing in ELL pyramidal neurons. In excellent agreement with immunohistochemistry, these effects were greatest in the LS and weakest in the CMS. Occlusion experiments revealed that 5-HT application inhibited both SK and M currents, leading to reduced rheobase current and increasing the *f-I* curve

Downloaded from jn.physiology.org on March 25, 2011

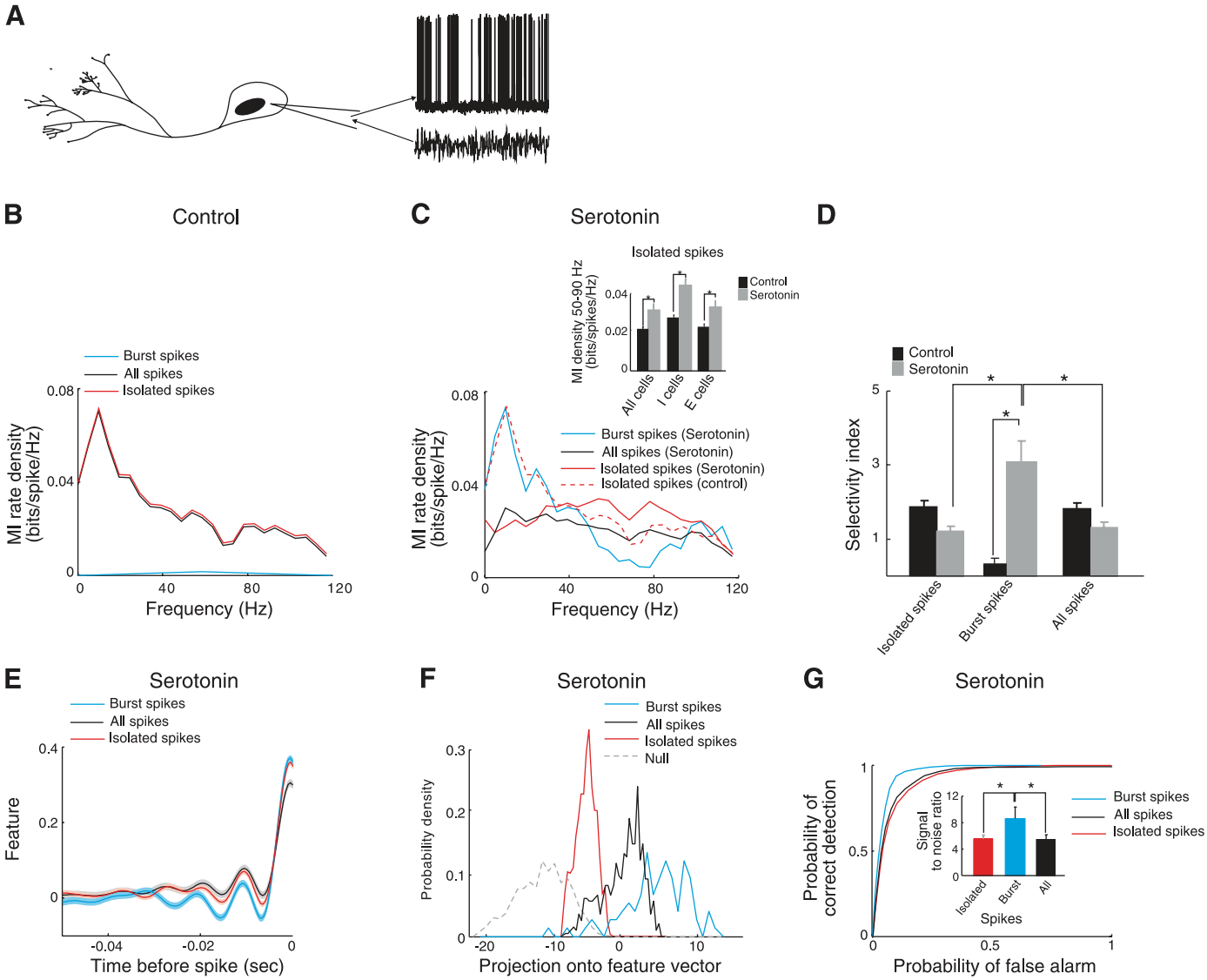

Fig. 9. 5-HT application induces feature detection by burst and information transmission by isolated spikes in ELL pyramidal neurons. *A*: schematic of the stimulation paradigm. A noise current was injected through the recording electrode and gave rise to a spiking response. *B*: mutual information (MI) rate density curves from a typical LS I-type pyramidal neuron obtained from all spikes, burst spikes, and isolated spikes under control conditions. *C*: MI rate density curves from the same neuron in *B* obtained from all spikes, burst spikes, and isolated spikes after 5-HT application. For comparison, the trace for isolated spikes in the control condition from *B* is also shown. *Inset* shows the change in MI density of isolated spikes over the midrange frequency in response to 5-HT for all cells as well as for E- and I-cells separately. *D*: selectivity index from all spikes, burst spikes, and isolated spikes under control conditions and after 5-HT application. 5-HT application led to significant increases in the selectivity index computed from burst events. Moreover, the selectivity index computed from burst events was significantly greater than that computed from either isolated spikes or all spikes. *E*: feature vectors obtained from all spikes, burst events, and isolated spikes from the same example neuron were relatively similar in shape. The lighter colored bands indicate the error as computed from bootstrapping. *F*: probability distributions $P(s/\lambda = 1)$ for bursts, isolated spikes, and all spikes, as well as the probability distribution $P(s/\lambda = 0)$ (i.e., the null distribution). The probability distribution for bursts shows the greatest degree of separation from the null distribution. *G*: receiver operating characteristic (ROC) curves obtained from all spikes, burst events, and isolated spikes from the same example neuron. *Inset*: signal-to-noise ratio (SNR) computed from all spikes, burst events, and isolated spikes. The SNR computed from burst events was significantly higher than those computed from isolated spikes or all spikes. Asterisks indicate statistical significance at the $P = 0.05$ level using a paired *t*-test.

gain in response to constant current stimulation. Although 5-HT application reduced the overall information rate, it induced increased burst firing, thereby enabling differential information transmission by different action potential patterns. Together with the fact that 5-HT application decreased the first spike latency to current steps, these results support the hypothesis that activating 5-HT input shifts ELL pyramidal cells to a burst-firing mode in which the bursts rapidly respond to and detect the presence of specific stimulus features while the isolated spikes transmit detailed information about different features. Further studies performed in vivo are necessary to verify this hypothesis and are beyond the scope of this article.

Serotonin Inhibits SK Currents in E-Cells: Implications for Gain Control

We have shown that 5-HT application increases E-cell excitability in part by reducing the SK current. This is, to our knowledge, the first demonstration that SK channels are inhibited by 5-HT in vertebrate sensory neurons. The distribution of

Downloaded from jn.physiology.org on March 25, 2011

SK channels in the electrosensory system is known (Ellis et al. 2008). Comparing our results to those of Ellis et al. (2008) reveals similar expression patterns across the ELL segments. In particular, both the SK1 and SK2 subtypes were found within the ELL with strongest expression in LS and weakest expression in CMS. In general, SK2 channels were located on E-cell somata, whereas SK1 channels were located on E- and I-cell dendrites. Since the effects of 5-HT were occluded by UCL only in E-cells, our results thus show that SK2 channels are inhibited by 5-HT. Such inhibition is likely to be widespread in sensory brain areas, because previous studies showed that SK channels are inhibited by 5-HT when coexpressed in oocytes (Grunnet et al. 2004).

5-HT also led to an increased *f-I* curve gain in E-cells through SK2 channel inhibition. Changes in the *f-I* curve gain constitute gain modulation, a phenomenon that is seen ubiquitously in the brain (Chance et al. 2002; Murphy and Miller 2003). We have shown the novel result that gain modulation can be implemented through SK channel regulation by 5-HT. Moreover, SK channels are expressed ubiquitously across the CNS and can regulate spike frequency adaptation, spike patterning, synaptic excitability, dendrosomatic coupling, and long-term potentiation (Bond et al. 2005; Faber and Sah 2002). As such, it is possible 5-HT regulates these functions in ELL as well as other systems, but the required studies are beyond the scope of this study.

Serotonin Inhibits M Currents in Both E- and I-Cells: Implications for Sensory Processing

Our results show that 5-HT inhibits a subthreshold potassium current that is blocked by the selective M current antagonists linopirdine and XE-991. As such, we have demonstrated for the first time that M currents are inhibited by 5-HT. These are expressed ubiquitously in the central nervous system (CNS) and regulate burst firing (Drion et al. 2010; Sotty et al. 2009; Yoshida and Alonso 2007; Yue and Yaari 2004). However, links between their kinetics and behaviorally relevant functions are poorly understood. Our results have shown that 5-HT, by inhibiting M currents, led to an increase in the rheobase current, thereby shifting the *f-I* curve of both E- and I-cells to the left, thus decreasing the first spike latency in response to current steps. We note that such changes in latency have been observed in vivo in other systems (Hurley and Pollak 2005b), and we propose that reduced M currents might be responsible for these.

5-HT Promotes Feature Detection by Bursts

5-HT application leads to increased burst firing in ELL pyramidal neurons. The functions of burst firing in ELL are well known and similar to those seen in other systems (Lesica and Stanley 2004; Lisman 1997; Sherman and Guillary 2002). They consist of feature detection (Gabbiani 1996; Metzner et al. 1998; Oswald et al. 2004) and the parallel coding of low- and high-frequency stimuli by bursts and isolated spikes (Oswald et al. 2004). Although 5-HT-induced burst firing had these functions, we have shown the novel result that isolated spikes carry 150% more information about higher temporal frequencies after 5-HT application. Because this effect was not seen previously when SK channel blockers were used (Ellis et al. 2007b), it is most likely due to M current inhibition by 5-HT.

We note that the discrimination performances of burst events, all spikes, and isolated spikes were quite good. This is most likely a consequence of the fact that our results were obtained in vitro, where neurons display much less trial-to-trial variability in their responses to sensory input (Stein et al. 2005). Indeed, the discrimination performances of burst events in vivo, while still higher than those of all spikes or isolated spikes, are much worse than in vitro (Oswald et al. 2004), and this is most likely due to increased trial-to-trial variability in vivo (Avila-Akerberg et al. 2010). It is thus likely that the improved discrimination performance of bursts induced by 5-HT would be of use to the organism, although studies performed in vivo are needed to verify this hypothesis.

Modulation of Intrinsic and Network Properties by 5-HT

It is important to note that because all our results were obtained in vitro, they solely pertain to the modulation of intrinsic ELL pyramidal cell properties. It is likely that these findings will hold in vivo, since ELL pyramidal neurons display similar tuning to current injection in vitro and sensory stimulation in vivo (Krahe et al. 2008; Mehaffey et al. 2008c). However, it is important to note that ELL pyramidal cells also receive massive feedback input from higher brain centers. In particular, they receive indirect parallel fiber input from cerebellar granule cells within the EGp that acts to modulate the ELL pyramidal cell responses to sensory input through changes in gain (Bastian 1986a,b) and by attenuating their responses to low-frequency input (Bastian et al. 2004; Chacron et al. 2005). It is quite likely that 5-HT can alter such feedback given the dense 5-HT staining observed in EGp. Studies performed in vivo are required to understand possible interactions between the effects of 5-HT on the intrinsic properties of ELL pyramidal cells and the effects of 5-HT on the feedback input that they receive.

Implications for Behavior

Serotonergic fibers derive from a small number of brain stem neurons yet innervate extensive regions of the vertebrate CNS (Brownfield et al. 1998; Johnston et al. 1990). For this reason, 5-HT has been considered as a modulator of an animal's internal "state," although this latter term remains poorly defined. In *A. leptorhynchus*, the 5-HT effects in ELL and in the control nucleus of electrocommunication (Johnston et al. 1990; Kawasaki et al. 1988; Smith and Combs 2008) appear to be related to the fish's aggressive and courtship behavior as well as associated sensory processing. Indeed, heightened 5-HT levels are observed in submissive individuals as opposed to dominant ones (Maler and Ellis 1987; Smith and Combs 2008). In *A. leptorhynchus*, interacting same-sex individuals produce low-frequency ($<$50 Hz) beats and high-frequency transient communication signals (i.e., chirps). However, interacting with opposite-sex individuals produces high-frequency ($>$50 Hz) beats (Zakon et al. 2002). Chirp stimuli are produced during both agonistic and courtship behaviors, and 5-HT injection will inhibit chirping (Maler and Ellis 1987; Smith and Combs 2008). Moreover, lesioning LS will also inhibit chirping (Metzner and Juranek 1997), and LS neurons display the strongest responses to chirps (Marsat et al. 2009; Metzner and

Downloaded from jn.physiology.org on March 25, 2011

Juranek 1997). 5-HT therefore most likely modulates pyramidal cell responses to stimuli that occur during such behavioral contexts.

Except for gain modulation, 5-HT affected E- and I-cells in a similar fashion. This is unlike what is seen in other systems, where 5-HT application can affect excitability and responses to sensory input in opposite fashion within the same brain area through activation of different 5-HT receptor subtypes (see Hurley et al. 2004 for review). This suggests that 5-HT has a unique function in ELL: heightened 5-HT levels may enable submissive individuals to better detect signal features that are associated with a dominant fish of the same sex, while at the same time being able to estimate the details of signals associated with a fish of the opposite sex. Indeed, previous results have shown that both E- and I-type LS pyramidal neurons will respond to low- and high-frequency beats with isolated spikes and respond to chirp stimuli with bursts of action potentials under control conditions (Krahe et al. 2008; Marsat and Maler 2010; Marsat et al. 2009). We predict that increased 5-HT levels will cause E- and I-type pyramidal neurons to now burst in response to both low-frequency beats and chirps, thereby providing a reliable signal that detects features associated with a dominant individual of the same sex. However, we also predict that these neurons will tend to better respond to higher frequency beats associated with individuals of the opposite sex with isolated spikes. As such, 5-HT would act to make both E- and I-type ELL pyramidal neurons more sensitive to these stimuli, thereby enhancing the animal's ability to detect these signals in a complex sensory environment. These hypotheses are highly speculative, and future studies performed in vivo are needed to verify these predictions. We note that burst firing by ELL pyramidal cells appears to be behaviorally relevant, because midbrain neurons that receive direct synaptic input from ELL respond specifically to these bursts (Fortune and Rose 1997).

Conclusion

In the present study, we have shown that 5-HT inhibits both M and SK-mediated currents, leading to gain modulation and parallel processing by different action potential patterns. Future studies should focus on other regions that receive 5-HT input, such as the midbrain (Johnston et al. 1990), as well as cerebellar granule cells providing feedback input to ELL (EGp, Fig. 1). Because the 5-HT system is highly conserved from teleost fish to mammals, the effects of 5-HT in ELL, midbrain, and EGp will likely directly address the general question as to the role of 5-HT in regulating sensory processing.

ACKNOWLEDGMENTS

We thank Eric S. Fortune and Gary Marsat for useful discussions.

GRANTS

This research was supported by Canadian Institutes of Health Research, Canada Foundation for Innovation, and Canada Research Chairs.

DISCLOSURES

No conflicts of interest, financial or otherwise, are declared by the author(s).

REFERENCES

Avila-Akerberg O, Krahe R, Chacron MJ. Neural heterogeneities and stimulus properties affect burst coding in vivo. *Neuroscience* 168: 300–313, 2010.

Bastian J. Gain control in the electrosensory system mediated by descending inputs to the electrosensory lateral line lobe. *J Neurosci* 6: 553–562, 1986a.

Bastian J. Gain control in the electrosensory system. A role for descending projections to the lateral electrosensory lateral line lobe. *J Comp Physiol A* 158: 505–515, 1986b.

Bastian J, Chacron MJ, Maler L. Plastic and non-plastic cells perform unique roles in a network capable of adaptive redundancy reduction. *Neuron* 41: 767–779, 2004.

Beique JC, Campbell B, Perring P, Hamblin MW, Walker P, Mladenovic L, Andrade R. Serotonergic regulation of membrane potential in developing rat prefrontal cortex: coordinated expression of 5-hydroxytryptamine (5-HT)1A, 5-HT2A, and 5-HT7 receptors. *J Neurosci* 24: 4807–4817, 2004.

Beique JC, Imad M, Mladenovic L, Gingrich JA, Andrade R. Mechanism of the 5-hydroxytryptamine 2A receptor-mediated facilitation of synaptic activity in prefrontal cortex. *Proc Natl Acad Sci USA* 104: 9870–9875, 2007.

Bell CC, Maler L. Central neuroanatomy of electrosensory systems in fish. In: *Springer Handbook of Auditory Research: Electroreception*. New York: Springer, 2005.

Berger M, Gray JA, Roth BL. The expanded biology of serotonin. *Annu Rev Med* 60: 355–366, 2009.

Berman NJ, Maler L. Distal versus proximal inhibitory shaping of feedback excitation in the electrosensory lateral line lobe: implications for sensory filtering. *J Neurophysiol* 80: 3214–3232, 1998a.

Berman NJ, Maler L. Inhibition evoked from primary afferents in the electrosensory lateral line lobe of the weakly electric fish (*Apteronotus leptorhynchus*). *J Neurophysiol* 80: 3173–3196, 1998b.

Berman NJ, Maler L. Interaction of $GABA_B$-mediated inhibition with voltage-gated currents of pyramidal cells: computational mechanism of a sensory searchlight. *J Neurophysiol* 80: 3197–3213, 1998c.

Bohorquez A, Hurley LM. Activation of serotonin 3 receptors changes in vivo auditory responses in the mouse inferior colliculus. *Hear Res* 251: 29–38, 2009.

Bond CT, Maylie J, Adelman JP. SK channels in excitability, pacemaking and synaptic integration. *Curr Opin Neurobiol* 15: 305–311, 2005.

Borst A, Haag J. Effects of mean firing on neural information rate. *J Comput Neurosci* 10: 213–221, 2001.

Borst A, Theunissen F. Information theory and neural coding. *Nat Neurosci* 2: 947–957, 1999.

Brenner R, Chen QH, Vilaythong A, Toney GM, Noebels JL, Aldrich RW. BK channel beta4 subunit reduces dentate gyrus excitability and protects against temporal lobe seizures. *Nat Neurosci* 8: 1752–1759, 2005.

Brownfield MS, Yracheta J, Chu F, Lorenz D, Diaz A. Functional chemical neuroanatomy of serotonergic neurons and their targets: antibody production and immunohistochemistry (IHC) for 5-HT, its precursor (5-HTP) and metabolite (5-HIAA), biosynthetic enzyme (TPH), transporter (SERT), and three receptors (5-HT2A, 5-ht5a, 5-HT7). *Ann NY Acad Sci* 861: 232–233, 1998.

Carr CE, Maler L, Sas E. Peripheral organization and central projections of the electrosensory organs in gymnotiform fish. *J Comp Neurol* 211: 139–153, 1982.

Chacron MJ, Longtin A, Maler L. The effects of spontaneous activity, background noise, and the stimulus ensemble on information transfer in neurons. *Network* 14: 803–824, 2003.

Chacron MJ, Maler L, Bastian J. Feedback and feedforward control of frequency tuning to naturalistic stimuli. *J Neurosci* 25: 5521–5532, 2005.

Chance FS, Abbott LF, Reyes AD. Gain modulation from background synaptic input. *Neuron* 35: 773–782, 2002.

Davison AC, Hinkley DV. *Bootstrap Methods and Their Application*. New York: Cambridge University Press, 2006.

Deng Q, Rashid AJ, Fernandez FR, Turner RW, Maler L, Dunn RJ. A C-terminal domain directs Kv3.3 channels to dendrites. *J Neurosci* 25: 11531–11541, 2005.

Doiron B, Chacron MJ, Maler L, Longtin A, Bastian J. Inhibitory feedback required for network oscillatory responses to communication but not prey stimuli. *Nature* 421: 539–543, 2003a.

Doiron B, Noonan L, Lemon N, Turner RW. Persistent Na^+ current modifies burst discharge by regulating conditional backpropagation of dendritic spikes. *J Neurophysiol* 89: 324–337, 2003b.

Downloaded from jn.physiology.org on March 25, 2011

Drion G, Bonjean M, Waroux O, Scuvee-Moreau J, Liegeois JF, Sejnowski TJ, Sepulchre R, Seutin V. M-type channels selectively control bursting in rat dopaminergic neurons. *Eur J Neurosci* 31: 827–835, 2010.

Ellis LD, Krahe R, Bourque CM, Dunn RJ, Chacron MJ. Muscarinic receptors control frequency tuning through the downregulation of an A-type potassium current. *J Neurophysiol* 98: 1526–1537, 2007a.

Ellis LD, Maler L, Dunn RJ. Differential distribution of SK channel subtypes in the brain of the weakly electric fish *Apteronotus leptorhynchus*. *J Comp Neurol* 507: 1964–1978, 2008.

Ellis LD, Mehaffey WH, Harvey-Girard E, Turner RW, Maler L, Dunn RJ. SK channels provide a novel mechanism for the control of frequency tuning in electrosensory neurons. *J Neurosci* 27: 9491–9502, 2007b.

Faber ES, Sah P. Physiological role of calcium-activated potassium currents in the rat lateral amygdala. *J Neurosci* 22: 1618–1628, 2002.

Foehring RC, van Brederode JF, Kinney GA, Spain WJ. Serotonergic modulation of supragranular neurons in rat sensorimotor cortex. *J Neurosci* 22: 8238–8250, 2002.

Fortune ES, Rose G. Passive and active membrane properties contribute to the temporal filtering properties of midbrain neurons in vivo. *J Neurosci* 17: 3815–3825, 1997.

Gabbiani F. Coding of time varying signals in spike trains of linear and half-wave rectifying neurons. *Network* 7: 61–85, 1996.

Gabbiani F, Metzner W, Wessel R, Koch C. From stimulus encoding to feature extraction in weakly electric fish. *Nature* 384: 564–567, 1996.

Gluais P, Edwards G, Weston AH, Falck JR, Vanhoutte PM, Feletou M. Role of SK_{Ca} and IK_{Ca} in endothelium-dependent hyperpolarizations of the guinea-pig isolated carotid artery. *Br J Pharmacol* 144: 477–485, 2005.

Green D, Swets J. *Signal Detection Theory and Psychophysics*. New York: John Wiley & Sons, 1966.

Grunnet M, Jespersen T, Perrier JF. 5-HT1A receptors modulate small-conductance Ca^{2+}-activated K^+ channels. *J Neurosci Res* 78: 845–854, 2004.

Gu N, Vervaeke K, Hu H, Storm JF. Kv7/KCNQ/M and HCN/h, but not KCa2/SK channels, contribute to the somatic medium after-hyperpolarization and excitability control in CA1 hippocampal pyramidal cells. *J Physiol* 566: 689–715, 2005.

Heiligenberg W. *Neural Nets in Electric Fish*. Cambridge, MA: MIT, 1991.

Heiligenberg W, Dye J. Labelling of electrosensory afferents in a gymnotid fish by intracellular injection of HRP: the mystery of multiple maps. *J Comp Physiol A* 148: 287–296, 1982.

Hilgers RH, Webb RC. Molecular aspects of arterial smooth muscle contraction: focus on Rho. *Exp Biol Med (Maywood)* 230: 829–835, 2005.

Hitschfeld EM, Stamper SA, Vonderschen K, Fortune ES, Chacron MJ. Effects of restraint and immobilization on electrosensory behaviors of weakly electric fish. *ILAR J* 50: 361–372, 2009.

Hosseini R, Benton DC, Dunn PM, Jenkinson DH, Moss GW. SK3 is an important component of K^+ channels mediating the afterhyperpolarization in cultured rat SCG neurones. *J Physiol* 535: 323–334, 2001.

Hupe GJ, Lewis JE, Benda J. The effect of difference frequency on electrocommunication: chirp production and encoding in a species of weakly electric fish, Apteronotus leptorhynchus. *J Physiol (Paris)* 102: 164–172, 2008.

Hurley LM. Different serotonin receptor agonists have distinct effects on sound-evoked responses in inferior colliculus. *J Neurophysiol* 96: 2177–2188, 2006.

Hurley LM, Devilbiss DM, Waterhouse BD. A matter of focus: monoaminergic modulation of stimulus coding in mammalian sensory networks. *Curr Opin Neurobiol* 14: 488–495, 2004.

Hurley LM, Pollak GD. Serotonin modulates responses to species-specific vocalizations in the inferior colliculus. *J Comp Physiol A Neuroethol Sens Neural Behav Physiol* 191: 535–546, 2005a.

Hurley LM, Pollak GD. Serotonin shifts first-spike latencies of inferior colliculus neurons. *J Neurosci* 25: 7876–7886, 2005b.

Johnston SA, Maler L, Tinner B. The distribution of serotonin in the brain of *Apteronotus leptorhynchus*: an immunohistochemical study. *J Chem Neuroanat* 3: 429–465, 1990.

Kawasaki M, Maler L, Rose G, Heiligenberg W. Anatomical and functional organization of the prepacemaker nucleus in gymnotiform electric fish: the accommodation of two behaviors in one nucleus. *J Comp Neurol* 276: 113–131, 1988.

Koyama S, Appel SB. Characterization of M-current in ventral tegmental area dopamine neurons. *J Neurophysiol* 96: 535–543, 2006.

Krahe R, Bastian J, Chacron MJ. Temporal processing across multiple topographic maps in the electrosensory system. *J Neurophysiol* 2008.

Krahe R, Gabbiani F. Burst Firing in Sensory Systems. *Nat Rev Neurosci* 5: 13–23, 2004.

Lerche C, Scherer CR, Seebohm G, Derst C, Wei AD, Busch AE, Steinmeyer K. Molecular cloning and functional expression of KCNQ5, a potassium channel subunit that may contribute to neuronal M-current diversity. *J Biol Chem* 275: 22395–22400, 2000.

Lesica NA, Stanley GB. Encoding of natural scene movies by tonic and burst spikes in the lateral geniculate nucleus. *J Neurosci* 24: 10731–10740, 2004.

Lisman JE. Bursts as a unit of neural information: making unreliable synapses reliable. *Trends Neurosci* 20: 38–43, 1997.

Maler L. Neural strategies for optimal processing of sensory signals. *Prog Brain Res* 165: 135–154, 2007.

Maler L. Receptive field organization across multiple electrosensory maps. I. Columnar organization and estimation of receptive field size. *J Comp Neurol* 516: 376–393, 2009a.

Maler L. Receptive field organization across multiple electrosensory maps. II. Computational analysis of the effects of receptive field size on prey localization. *J Comp Neurol* 516: 394–422, 2009b.

Maler L. The posterior lateral line lobe of certain gymnotiform fish. Quantitative light microscopy. *J Comp Neurol* 183: 323–363, 1979.

Maler L, Ellis WG. Inter-male aggressive signals in weakly electric fish are modulated by monoamines. *Behav Brain Res* 25: 75–81, 1987.

Maler L, Finger T, Katen HJ. Differential projections of ordinary lateral line and electroreceptors in the gymnotiform fish, *Apternotus albifrons*. *J Comp Neurol* 158: 363–382, 1974.

Maler L, Mugnaini E. Correlating gamma-aminobutyric acidergic circuits and sensory function in the electrosensory lateral line lobe of a gymnotiform fish. *J Comp Neurol* 345: 224–252, 1994.

Maler L, Sas E, Johnston S, Ellis W. An atlas of the brain of the weakly electric fish *Apteronotus leptorhynchus*. *J Chem Neuroanat* 4: 1–38, 1991.

Maler L, Sas EK, Rogers J. The cytology of the posterior lateral line lobe of high frequency weakly electric fish (*Gymnotoidei)*: differentiation and synaptic specificity in a simple cortex. *J Comp Neurol* 195: 87–139, 1981.

Marsat G, Maler L. Neural heterogeneity and efficient population codes for communication signals. *J Neurophysiol* 104: 2543–2555, 2010.

Marsat G, Proville RD, Maler L. Transient signals trigger synchronous bursts in an identified population of neurons. *J Neurophysiol* 102: 714–723, 2009.

Mathieson WB, Heiligenberg W, Maler L. Ultrastructural studies of physiologically identified electrosensory afferent synapses in the gymnotiform fish, *Eigenmannia*. *J Comp Neurol* 255: 526–537, 1987.

Mathieson WB, Maler L. Morphological and electrophysiological properties of a novel in vitro preparation: the electrosensory lateral line lobe brain slice. *J Comp Physiol A* 163: 489–506, 1988.

Matthews EA, Weible AP, Shah S, Disterhoft JF. The BK-mediated fAHP is modulated by learning a hippocampus-dependent task. *Proc Natl Acad Sci USA* 105: 15154–15159, 2008.

Mehaffey WH, Doiron B, Maler L, Turner RW. Deterministic multiplicative gain control with active dendrites. *J Neurosci* 25: 9968–9977, 2005.

Mehaffey WH, Ellis LD, Krahe R, Dunn RJ, Chacron MJ. Ionic and neuromodulatory regulation of burst discharge controls frequency tuning. *J Physiol (Paris)* 102: 195–208, 2008a.

Mehaffey WH, Fernandez FR, Doiron B, Turner RW. Regulation of somatic firing dynamics by backpropagating dendritic spikes. *J Physiol (Paris)* 102: 181–194, 2008b.

Mehaffey WH, Maler L, Turner RW. Intrinsic frequency tuning in ELL pyramidal cells varies across electrosensory maps. *J Neurophysiol* 99: 2641–2655, 2008c.

Metzner W, Juranek J. A sensory brain map for each behavior? *Proc Natl Acad Sci USA* 94: 14798–14803, 1997.

Metzner W, Koch C, Wessel R, Gabbiani F. Feature extraction by burst-like spike patterns in multiple sensory maps. *J Neurosci* 18: 2283–2300, 1998.

Middleton JW, Longtin A, Benda J, Maler L. The cellular basis for parallel neural transmission of a high-frequency stimulus and its low-frequency envelope. *Proc Natl Acad Sci USA* 103: 14596–14601, 2006.

Monaghan AS, Benton DC, Bahia PK, Hosseini R, Shah YA, Haylett DG, Moss GW. The SK3 subunit of small conductance Ca^{2+}-activated K^+ channels interacts with both SK1 and SK2 subunits in a heterologous expression system. *J Biol Chem* 279: 1003–1009, 2004.

Murphy BK, Miller KD. Multiplicative gain changes are induced by excitation or inhibition alone. *J Neurosci* 23: 10040–10051, 2003.

Oswald AM, Chacron MJ, Doiron B, Bastian J, Maler L. Parallel processing of sensory input by bursts and isolated spikes. *J Neurosci* 24: 4351–4362, 2004.

Downloaded from jn.physiology.org on March 25, 2011

Oswald AM, Doiron B, Maler L. Interval coding. I. Burst interspike intervals as indicators of stimulus intensity. *J Neurophysiol* 97: 2731–2743, 2007.

Pineda JC, Galarraga E, Foehring RC. Different Ca^{2+} source for slow AHP in completely adapting and repetitive firing pyramidal neurons. *Neuroreport* 10: 1951–1956, 1999.

Rieke F, Warland D, de Ruyter van Steveninck RR, Bialek W. *Spikes: Exploring the Neural Code*. Cambridge, MA: MIT, 1996.

Sadeghi SG, Chacron MJ, Taylor MC, Cullen KE. Neural variability, detection thresholds, and information transmission in the vestibular system. *J Neurosci* 27: 771–781, 2007.

Sah P. Ca^{2+}-activated K^+ currents in neurones: types, physiological roles and modulation. *Trends Neurosci* 19: 150–154, 1996.

Sas E, Maler L. The nucleus praeeminentialis: a Golgi study of a feedback center in the electrosensory system of gymnotid fish. *J Comp Neurol* 221: 127–144, 1983.

Sas E, Maler L. The organization of afferent input to the caudal lobe of the cerebellum of the gymnotid fish *Apteronotus leptorhynchus*. *Anat Embryol (Berl)* 177: 55–79, 1987.

Sas E, Maler L. Somatostatin-like immunoreactivity in the brain of an electric fish (*Apteronotus leptorhynchus*) identified with monoclonal antibodies. *J Chem Neuroanat* 4: 155–186, 1991.

Saunders J, Bastian J. The physiology and morphology of two classes of electrosensory neurons in the weakly electric fish *Apteronotus Leptorhynchus*. *J Comp Physiol A* 154: 199–209, 1984.

Schwindt PC, Spain WJ, Crill WE. Long-lasting reduction of excitability by a sodium-dependent potassium current in cat neocortical neurons. *J Neurophysiol* 61: 233–244, 1989.

Shah MM, Mistry M, Marsh SJ, Brown DA, Delmas P. Molecular correlates of the M-current in cultured rat hippocampal neurons. *J Physiol* 544: 29–37, 2002.

Shannon CE. A mathematical theory of communication. *Bell System Tech J* 27: 379–423, 623–656, 1948.

Shapiro MS, Roche JP, Kaftan EJ, Cruzblanca H, Mackie K, Hille B. Reconstitution of muscarinic modulation of the KCNQ2/KCNQ3 K^+ channels that underlie the neuronal M current. *J Neurosci* 20: 1710–1721, 2000.

Shen KZ, Kozell LB, Johnson SW. Multiple conductances are modulated by 5-HT receptor subtypes in rat subthalamic nucleus neurons. *Neuroscience* 148: 996–1003, 2007.

Sherman SM. Tonic and burst firing: dual modes of thalamocortical relay. *Trends Neurosci* 24: 122–126, 2001.

Sherman SM, Guillary RW. The role of the thalamus in the flow of information to the cortex. *Philos Trans R Soc Lond B Biol Sci* 357: 1695–1708, 2002.

Shumway C. Multiple electrosensory maps in the medulla of weakly electric Gymnotiform fish. I. Physiological differences. *J Neurosci* 9: 4388–4399, 1989a.

Shumway C. Multiple electrosensory maps in the medulla of weakly electric Gymnotiform fish. II. Anatomical differences. *J Neurosci* 9: 4400–4415, 1989b.

Smith GT, Combs N. Serotonergic activation of 5HT1A and 5HT2 receptors modulates sexually dimorphic communication signals in the weakly electric fish *Apteronotus leptorhynchus*. *Horm Behav* 54: 69–82, 2008.

Smith GT, Unguez GA, Weber CM. Distribution of Kv1-like potassium channels in the electromotor and electrosensory systems of the weakly electric fish *Apteronotus leptorhynchus*. *J Neurobiol* 66: 1011–1031, 2006.

Sogaard R, Ljungstrom T, Pedersen KA, Olesen SP, Jensen BS. KCNQ4 channels expressed in mammalian cells: functional characteristics and pharmacology. *Am J Physiol Cell Physiol* 280: C859–C866, 2001.

Sotty F, Damgaard T, Montezinho LP, Mork A, Olsen CK, Bundgaard C, Husum H. Antipsychotic-like effect of retigabine [*N*-(2-amino-4-(fluorobenzylamino)-phenyl)carbamic acid ester], a KCNQ potassium channel opener, via modulation of mesolimbic dopaminergic neurotransmission. *J Pharmacol Exp Ther* 328: 951–962, 2009.

Stein RB, Gossen ER, Jones KE. Neuronal variability: noise or part of the signal? *Nat Rev Neurosci* 6: 389–397, 2005.

Telgkamp P, Combs N, Smith GT. Serotonin in a diencephalic nucleus controlling communication in an electric fish: sexual dimorphism and relationship to indicators of dominance. *Dev Neurobiol* 67: 339–354, 2007.

Toporikova N, Chacron MJ. SK channels gate information processing in vivo by regulating an intrinsic bursting mechanism seen in vitro. *J Neurophysiol* 102: 2273–2287, 2009.

Turner RW, Maler L, Burrows M. Electroreception and electrocommunication. *J Exp Biol* 202: 1167–1458, 1999.

Turner RW, Maler L, Deerinck T, Levinson SR, Ellisman MH. TTX-sensitive dendritic sodium channels underlie oscillatory discharge in a vertebrate sensory neuron. *J Neurosci* 14: 6453–6471, 1994.

Turner RW, Plant JR, Maler L. Oscillatory and burst discharge across electrosensory topographic maps. *J Neurophysiol* 76: 2364–2382, 1996.

Villalobos C, Beique JC, Gingrich JA, Andrade R. Serotonergic regulation of calcium-activated potassium currents in rodent prefrontal cortex. *Eur J Neurosci* 22: 1120–1126, 2005.

Villalobos CA, Bull P, Saez P, Cassels BK, Huidobro-Toro JP. 4-Bromo-2,5-dimethoxyphenethylamine (2C-B) and structurally related phenylethylamines are potent 5-HT2A receptor antagonists in *Xenopus laevis* oocytes. *Br J Pharmacol* 141: 1167–1174, 2004.

Waterhouse BD, Azizi SA, Burne RA, Woodward DJ. Modulation of rat cortical area 17 neuronal responses to moving visual stimuli during norepinephrine and serotonin microiontophoresis. *Brain Res* 514: 276–292, 1990.

Waterhouse BD, Moises HC, Woodward DJ. Interaction of serotonin with somatosensory cortical neuronal responses to afferent synaptic inputs and putative neurotransmitters. *Brain Res Bull* 17: 507–518, 1986.

Yoshida M, Alonso A. Cell-type specific modulation of intrinsic firing properties and subthreshold membrane oscillations by the M(Kv7)-current in neurons of the entorhinal cortex. *J Neurophysiol* 98: 2779–2794, 2007.

Yuan Q, Harley CW, McLean JH. Mitral cell beta1 and 5-HT2A receptor colocalization and cAMP coregulation: a new model of norepinephrine-induced learning in the olfactory bulb. *Learn Mem* 10: 5–15, 2003.

Yue C, Yaari Y. Axo-somatic and apical dendritic Kv7/M channels differentially regulate the intrinsic excitability of adult rat CA1 pyramidal cells. *J Neurophysiol* 95: 3480–3495, 2006.

Yue C, Yaari Y. KCNQ/M channels control spike afterdepolarization and burst generation in hippocampal neurons. *J Neurosci* 24: 4614–4624, 2004.

Zakon HH, Oestreich J, Tallarovic S, Triefenbach F. EOD modulations of brown ghost electric fish: JARs, chirps, rises, and dips. *J Physiol (Paris)* 96: 451–458, 2002.

Downloaded from jn.physiology.org on March 25, 2011